

1 **Crack models of repeating earthquakes predict observed**
2 **moment-recurrence scaling**

3 **C. Cattania^{1,2}, P.Segall¹**

4 ¹Department of Geophysics, Stanford University, Stanford, CA

5 ²GFZ German Research Centre for Geosciences, Potsdam, Germany

6 **Key Points:**

- 7 • Analytical expressions for recurrence interval and stress drop of events on circular as-
- 8 perities in creeping faults
- 9 • The theory produces the observed scaling between recurrence interval and seismic mo-
- 10 ment of repeating earthquakes
- 11 • We predict and quantify a break in self similarity and decrease in stress drops close to
- 12 the nucleation dimension

Abstract

Small repeating earthquakes are thought to represent rupture of isolated asperities loaded by surrounding creep. The observed scaling between recurrence interval and seismic moment, $T_r \sim M^{1/6}$, contrasts with expectation assuming constant stress drop and no aseismic slip ($T_r \sim M^{1/3}$). Here we demonstrate that simple crack models of velocity-weakening asperities in a velocity-strengthening fault predict the $M^{1/6}$ scaling; however, the mechanism depends on asperity radius, R . For small asperities ($R_\infty < R < 2R_\infty$, where R_∞ is the nucleation radius) numerical simulations with rate-state friction show interseismic creep penetrating inwards from the edge, earthquakes nucleate in the center and rupture the entire asperity. Creep penetration accounts for $\sim 25\%$ of the slip budget, the nucleation phase takes up a larger fraction of slip. Stress drop increases with increasing R ; the lack of self-similarity being due to the finite nucleation dimension.

For $2R_\infty < R \lesssim 6R_\infty$ simulations exhibit simple cycles with ruptures nucleating from the edge. Asperities with $R \gtrsim 6R_\infty$ exhibit complex cycles of partial and full ruptures. Here T_r is explained by an energy criterion: full rupture requires that the energy release rate everywhere on the asperity at least equals the fracture energy, leading to the scaling $T_r \sim M^{1/6}$. Remarkably, in spite of the variability in behavior with source dimension, the scaling of T_r with stress drop $\Delta\tau$, nucleation length and creep rate v_{pl} is the same across all regimes: $T_r \sim \sqrt{R_\infty} \Delta\tau^{5/6} M_0^{1/6} / v_{pl}$. This supports the use of repeating earthquakes as creepmeters, and provides a physical interpretation for the scaling observed in nature.

1 Plain language summary

While most earthquake sequences have complex temporal patterns, some small earthquakes are quite predictable: they repeat periodically. The time between consecutive events (recurrence interval) grows with earthquake size: as intuitive, it takes longer to accumulate the potential energy for large earthquakes. However, the scaling between the recurrence interval and earthquake energy (seismic moment) is not what simple physical considerations predict. It is often assumed that faults are locked between events and seismic slip must therefore keep up with long term plate motion. This leads to the scaling: $T_r \sim M_0^{1/3}$, but the observed scaling is $T_r \sim M_0^{1/6}$.

In fact, faults are not fully locked between earthquakes: they can slip slowly, or release part of the energy in smaller quakes between the larger ones. Here we use numerical simulations, and ideas from fracture mechanics, to understand what controls the time between re-

45 peating quakes. The main results are: (1) analytical expressions of the recurrence interval as
 46 a function of earthquake size, predicting the observed scaling; (2) explanation of the differ-
 47 ences between the cycle of small and large earthquakes (fraction of slow slip, direction of rup-
 48 ture propagation, and the occurrence of smaller quakes between large ones) and the quanti-
 49 ties determining these transitions.

50 2 Introduction

51 Unlike large earthquakes, small quakes can be very predictable; periodic sequences of
 52 events with very similar waveforms have been detected in multiple locations worldwide. They
 53 are typically understood as the rupture of locked patches surrounded by aseismic creep load-
 54 ing them at a usually constant rate. An interesting observation is the scaling between their re-
 55 currence interval and seismic moment. *Nadeau and Johnson* [1998] observed that the recur-
 56 rence interval T_r and seismic moment M_0 scale as $T \sim M_0^{1/6}$ for small repeaters on the San
 57 Andreas fault, and subsequent studies confirmed this scaling in other areas [*Chen et al.*, 2007].
 58 As outlined by *Nadeau and Johnson* [1998], standard scaling arguments predict that $T_r \sim M_0^{1/3}$.
 59 Assuming constant stress drop constrains seismic slip to be linear with rupture dimension ($S \sim$
 60 R); further assuming that the coseismic slip is equal to the slip deficit accumulated since the
 61 previous event ($S = v_{pl}T_r$, where v_{pl} is fault slip rate) results in a linear scaling between
 62 recurrence interval T_r and R . Since $M_0 \sim \Delta\sigma R^3$ a constant stress drop $\Delta\sigma$ implies $T_r \sim$
 63 $M_0^{1/3}$. *Nadeau and Johnson* [1998] explained the observed scaling by abandoning the constant
 64 stress drop assumption, inferring $\Delta\sigma \sim M_0^{-1/4}$. To fit observations, very high stress drops
 65 (of the order of 10^3 – 10^4 MPa) are required for the smallest events. Alternatively, the scal-
 66 ing can be explained by assuming constant $\Delta\sigma$ but relaxing the assumption that $S = v_{pl}T_r$,
 67 that is, by not assuming that the fault is entirely locked interseismically so that the coseismic
 68 slip is less than $v_{pl}T_r$. This was suggested by *Beeler et al.* [2001], who adopted a strain-hardening
 69 rheology on a circular patch experiencing spatially uniform interseismic creep. According to
 70 their model, smaller asperities release a large fraction of slip aseismically, which can result
 71 in the observed scaling. Similar conclusions were reached by *Chen and Lapusta* [2009], who
 72 presented numerical simulations of seismic cycles on circular, velocity-weakening asperities
 73 surrounded by a velocity strengthening exterior. They found that smaller asperities experience
 74 a larger fraction of aseismic slip, as suggested by *Beeler et al.* [2001]. Alternatively, *Sammis*
 75 *and Rice* [2001] proposed a geometrical explanation: asperities at the transition between locked
 76 and creeping regions experience a stress field decaying with distance from the transition, which

77 under certain assumptions results in $T_r \sim M_0^{1/6}$. Because of the particular geometry, this may
 78 be less generally applicable than the aseismic slip interpretation.

Here we seek a deeper understanding of the factors that control the recurrence interval of earthquakes on circular asperities using fracture mechanics concepts, guided by numerical simulations of faults obeying rate-state friction. *Chen and Lapusta* [2009] demonstrated that numerical simulations of velocity weakening asperities embedded in a velocity strengthening fault reproduce the $T_r \sim M_0^{1/6}$ scaling. They attributed this observation to the occurrence of creep, which is significant on asperities with a dimension close to the nucleation size. Here we start from a similar set of numerical simulations and derive analytical expressions for the recurrence interval. Our goal is twofold: first, by formulating the problem in terms of physical quantities such as stress drop and nucleation length, we develop a model which can be applied to a different choice of parameters or even a potentially different frictional behavior. Second, we explore the behavior of asperities much larger than the nucleation dimension, that do not experience significant aseismic slip. In this regime, we provide a different physical explanation for the observed scaling. The seismic moment of a circular crack of radius R with uniform stress drop $\Delta\sigma$ is [*Eshelby*, 1957]

$$M_0 = \frac{16}{7} \Delta\sigma R^3 \quad (1)$$

79 For constant stress drop, the scaling $T_r \sim M_0^{1/6}$ implies that $T_r \sim R^{1/2}$. Interestingly, this
 80 is analogous to the scaling derived by *Werner and Rubin* [2013] for antiplane faults, by con-
 81 sidering the balance between the energy release rate for a crack loaded by downdip creep and
 82 the fracture energy absorbed to propagate the crack through the full velocity weakening re-
 83 gion, and confirmed by *Kato* [2012a] for subduction zones. Here we demonstrate that, under
 84 certain assumptions, this energy argument applied to circular asperities leads to the analogous
 85 scaling for circular cracks. However, numerical simulations only exhibit this scaling above a
 86 critical radius (twice the nucleation radius R_∞ , defined below), and stress drop is not constant
 87 for asperities smaller than this dimension. We develop crack models to answer the following
 88 questions: (1) how long does it take for creep loading to nucleate a dynamic rupture? (2) once
 89 an event nucleates, under what conditions will it rupture the entire asperity? (3) how does stress
 90 drop vary with asperity dimension? We find that the answers to these questions depend on the
 91 asperity dimension R relative to R_∞ . This is perhaps not surprising, since this dimension con-
 92 trols the transition between aseismic and seismic slip; the occurrence of creep affects the strength
 93 of the asperity and hence rupture propagation. Furthermore, as R decreases towards R_∞ , the
 94 assumptions behind classical seismological models of circular ruptures break down: the rup-

95 ture cannot be assumed to start at a point expanding subsequently to seismic rupture veloc-
 96 ities. In this limit, the rupture is not self similar and the stress drop increases slightly with R .
 97 Combining these results, we obtain analytical estimates for the recurrence interval as a func-
 98 tion of asperity radius R , which predict a scaling close to that observed in nature. In summary,
 99 we show that T_r scales approximately with $M_0^{1/6}$ over a range of asperity radii, and poten-
 100 tially also for $R \gg R_\infty$; however the underlying physics differs depending on asperity size.

101 3 Numerical simulations

102 In order to test the analytical results derived in the next section, we ran a set of simu-
 103 lations analogous to those presented by *Chen and Lapusta* [2009]: a circular velocity-weakening
 104 asperity on an otherwise velocity-strengthening planar fault. Here we use the quasi-dynamic
 105 rupture code *FDRA* [*Segall and Bradley*, 2012; *Mavrommatis et al.*, 2017]. The agreement be-
 106 tween our simulation results and the fully dynamic models used by *Chen and Lapusta* [2009],
 107 and the success of our quasi-static derivations in reproducing the observed scaling, indicate
 108 that dynamic effects are not essential in determining the recurrence interval scaling.

The frictional resistance on the fault τ_f is controlled by rate-state friction [*Dieterich*, 1978]:

$$\tau_f(v, \theta) = \sigma \left[f_0 + a \log \frac{v}{v_0} + b \log \frac{\theta v_0}{d_c} \right], \quad (2)$$

where σ is effective the normal stress; a , b and are constitutive parameters; d_c is the rate-state
 slip-weakening distance (a characteristic sliding length over which state θ evolves). v and v_0
 are the slip velocity and a reference slip velocity; f_0 is the steady-state friction coefficient at
 $v = v_0$, and θ is a state-variable which here evolves according to the ageing law [*Ruina*, 1983]:

$$\frac{d\theta}{dt} = 1 - \frac{\theta v}{d_c}, \quad (3)$$

so that the steady-state strength at constant slip velocity v is given by

$$\tau_{ss}(v) = \sigma \left[f_0 + (a - b) \log \frac{v}{v_0} \right]. \quad (4)$$

109 *Chen* [2012] ran simulations with another commonly used state evolution law (the slip law),
 110 and showed that the scaling between recurrence interval and moment ($T_r \sim M_0^{1/6}$) is un-
 111 changed.

Slip on the fault is controlled by the following equation of motion:

$$\tau_{el}(\mathbf{x}) - \tau_f(\mathbf{x}) = \frac{\mu}{2c_s} v(\mathbf{x}), \quad (5)$$

112 where μ is the shear modulus and τ_{el} is the elastostatic shear stress due to loading from the
 113 boundary and quasi-static elastic interactions between fault elements computed through a Bound-
 114 ary Element Method (BEM) approach. The right hand side represents radiation damping, which
 115 accounts for the stress change due to radiation of plane S-waves [Rice, 1993], with c_s the shear
 116 wave speed.

Rate-state friction combined with elasticity leads to characteristic dimensions which con-
 trol earthquake nucleation, and the transition between seismic and aseismic behavior. One such
 dimension is

$$L_b = \frac{\mu' d_c}{\sigma b}. \quad (6)$$

117 where $\mu' = \mu$ for antiplane shear and $\mu/(1 - \nu)$, with $\nu =$ Poisson's ratio, for plane strain
 118 deformation. This length scale was first identified by Dieterich [1992] as the minimum nu-
 119 cleation length, although subsequent studies obtained different estimates [Rubin and Ampuero,
 120 2005, and references therein]. For nominal calculations we set $\mu = 30$ GPa, $\nu = 0.25$, $d_c =$
 121 0.1 mm, $b = 0.02$ and $a - b = \pm 0.005$ for the velocity strengthening and weakening region
 122 respectively, resulting in $L_b = 4$ m (antiplane shear), but later vary a/b . We tested asperity
 123 radii R such that R/L_b is between 6 and 100. The system is driven by imposed velocity $v =$
 124 v_{pl} (10^{-9} m/s) outside the domain, which has a size of $6R$ in each direction. As long as the
 125 domain boundaries are sufficiently far, the domain size has little influence of the simulation
 126 results: we tested sizes between $6R$ and $100R$ and found a variation of less than 1% in re-
 127 currence interval. We define earthquakes as the period during which the slip velocity at any
 128 point exceeds the threshold velocity $v_{dyn} = 2a\sigma c_s/\mu'$ (here 0.14 m/s) at which point the in-
 129 ertial term in Eq. 5 becomes significant [Rubin and Ampuero, 2005].

130 The rupture behavior as a function of R is described in detail in Chen and Lapusta [2009];
 131 here we summarize the main results. The smallest faults ($R \leq 12.5L_b$) are entirely aseismic.
 132 However, they also exhibit cycles: most slip takes place during short episodes of slip at a rate
 133 higher than loading rate (e.g. $v \sim 10^3 v_{pl}$ for the smallest fault, $R = 6L_b$), and are nearly
 134 locked between such events. Intermediate size asperities ($15.7L_b \leq R \leq 20.5L_b$) exhibit
 135 cycles of seismic ruptures nucleating at the center of the asperity (Fig. 1). After each rupture,
 136 a creep front propagates inwards from the edge, and the next rupture occurs when the front
 137 reaches the center. For larger asperities ($R \geq 25L_b$) ruptures nucleate from the side, when
 138 the creep front has only partially penetrated the asperity. There are always one or more tran-
 139 sient aseismic slip events in each cycle before reaching seismic velocities (Fig. 2). For $R \simeq$
 140 $22L_b$, central and lateral ruptures alternate. Finally, we note that on the largest asperity tested

141 ($R = 100L_b$) some seismic ruptures arrest before covering the entire asperity; we denote these
 142 as partial ruptures. We further explore the partial ruptures regime by choosing rate-state pa-
 143 rameters such that similar behavior can be reproduced with lower computational costs. As ex-
 144 pected, our simulations result in the $T_r \sim M_0^{1/6}$ scaling observed by *Chen and Lapusta* [2009]
 145 (Fig. 3), across all the regimes of seismic ruptures described above. However, Fig. 4 shows
 146 that the scaling between T_r and R varies with asperity radius. For seismic ruptures nucleat-
 147 ing at the center, $T_r \sim R$; whereas on asperities with lateral ruptures $T_r \sim R^{1/2}$ (consis-
 148 tent with $T_r \sim M_0^{1/6}$ scaling and constant stress drop). Aseismic events have shorter T_r com-
 149 pared to seismic central ruptures. In the following sections, we develop crack models to un-
 150 derstand the scaling of T_r with R (section 5.1) and the variation of stress drop with asperity
 151 dimension (section 6).

152 **4 Estimating $T_r(R)$ from crack models**

We estimate the recurrence interval by treating aseismic and seismic slip on the asperity as cracks, and determine their propagation or arrest based on energy balance concepts [e.g. *Griffith*, 1921; *Freund*, 1990]. This approach is analogous to the estimation of the critical nucleation length by *Rubin and Ampuero* [2005] and to the estimation of recurrence interval on vertical antiplane faults by *Werner and Rubin* [2013]. As shown by *Irwin* [1957], these energy criteria can be expressed in terms of stress intensity factors (SIF). We consider the following contributions to the SIF, K : (1) K_l , the stress intensity factor of a stress-free crack subject to external loading (creeping surrounding the asperity); (2) $K_{\Delta\tau}$ the stress intensity factor due to changes in stress within the crack due to the variation in strength with slip velocity. A crack can grow if the total stress intensity factor is at least equal to the toughness K_c :

$$K_l + K_{\Delta\tau} \geq K_c, \quad (7)$$

where K_c is related to the fracture energy G_c by

$$K_c = \sqrt{2\mu'G_c} \quad (8)$$

153 following the convention of *Tada et al.* [2000]. We use this framework to model two phases
 154 of slip on the fault: the interseismic inward propagation of the creep front, and the propaga-
 155 tion or arrest of a seismic rupture. Eq. 7 takes on two limiting cases: considering inward growth
 156 of the creeping zone, the slip speed immediately behind the crack tip is small (e.g. close to
 157 plate rate), thus the fracture energy, and hence K_c , is small, and $K_l \simeq -K_{\Delta\tau}$. On the other
 158 hand, considering the energy balance during a full seismic cycle, the total stress change $\Delta\tau =$

159 0 and Eq. 7 becomes $K_l = K_c$ (this is the argument introduced by *Werner and Rubin* [2013]
 160 to estimate T_r for vertical antiplane faults). As shown in the following section, these processes
 161 define two timescales: the time required for nucleation (T_{nucl}), and the time when a rupture
 162 can propagate over the full asperity (T_{full}).

163 5 Creep front propagation

164 5.1 Small asperities (central ruptures)

First we consider asperities small enough that the creep front reaches the center. Fig. 5(a,b) shows the propagation of the creep front for asperities of different sizes: Fig. 5b shows that the lines collapse to the same curve when both position and distance are normalized by a factor proportional to R . In appendix A, we estimate the equation of motion for the creep front by numerically solving Eq. 7 for an annular crack, with stress change given by the increase from a residual steady-state stress at coseismic slip speed $\tau_{ss}(v_{co})$ to steady-state friction at the fault slip-rate $\tau_{ss}(v_{pl})$, that is $\Delta\tau = \tau_{ss}(v_{pl}) - \tau_{ss}(v_{co})$, see Fig. 5(c). The black and dotted lines in Fig. 5(b) are the expected position of the front, with and without the contribution from fracture energy. Overall this model explains the creeping front propagation reasonably well, with a few differences: (1) early in the cycle, the creeping front propagates faster than expected, due to afterslip in the velocity strengthening region loading the fault faster than plate velocity; (2) towards the end of the cycle, the crack slips faster than expected, due to stressing from the opposing creep front, while our model assumes creep at $v = v_{pl}$. In appendix A we find that, neglecting fracture energy, the time required for creep to reach the center and nucleate a rupture is

$$T_{nucl}(R) = \frac{4\Delta\tau R}{\pi\mu'v_{pl}} \equiv R/\dot{r}_c. \quad (9)$$

where we introduced the characteristic speed for the creep front propagation $\dot{r}_c = \pi\mu'v_{pl}/4\Delta\tau$. The numerical solution is close to the following expression (derived in appendix A):

$$a(t) = R\sqrt{1 - t\dot{r}_c/R} \quad (10)$$

165 where a is the distance of the crack from the center; eq. 10 is shown by the dashed red line
 166 in Fig. 5b. As the crack approaches the center, its propagation speed and slip velocity increase
 167 and eventually the latter reaches v_{dyn} . For the smallest asperities simulated, we see a brief elas-
 168 todynamic event that decays as it expands outward before reaching the edge of the asperity
 169 (Fig. 1a, 7); these short rupture events are followed by a crack-like rupture expanding to the
 170 edge of the asperity. Since the moment of the second event is 1 to 2 orders of magnitude larger

171 than the initial acceleration (as can be seen from the slip profiles in Fig. 1) we consider the
 172 second event to be the repeating earthquake. This earthquake is well described as a constant
 173 stress drop crack propagating into the creeping region, where the stress is nearly uniform and
 174 equal to the steady state strength at v_{pl} , i.e., $\tau_{ss}(v_{pl})$. The stress intensity factor of an ellip-
 175 tical crack in a uniform stress field is an increasing function of its size [e.g. *Madariaga, 1977*].
 176 Therefore, once nucleated the ruptures tend to accelerate and expand until they reach the edge
 177 of the asperity. As seen in the simulations, all accelerating events on faults nucleating from
 178 the center result in full ruptures, or they are followed by a full rupture within a short time in-
 179 terval (3-8 orders of magnitude shorter than the cycle duration, as seen in Fig. 1), so that in
 180 this regime the recurrence interval is determined by T_{nucl} . The linear trend in T_r vs. R (Fig-
 181 ures 4 and 6) is in agreement with eq. 9. For even smaller (aseismic) asperities, we expect a
 182 similar behavior, with v_{co} replaced by the slip speed during slow events. This speed, and hence
 183 $\Delta\tau$, decreases for smaller asperities, which explains why aseismic faults ($R/L_b < 12.5$) have
 184 shorter T_r than expected from eq. 9 calculated with $\Delta\tau = \tau_{ss}(v_{pl}) - \tau_{ss}(v_{co})$ for seismic
 185 slip speeds (Fig. 4).

186 We test the dependence of this scaling on rate-state parameters by running simulations
 187 with the same ratio R/R_∞ (where R_∞ is the nucleation radius, defined in eq. 12), fixed b and
 188 variable a/b (Fig. 7). We observe essentially the same behavior, and the scaling predicted by
 189 eq. 9 for a/b between 0.3 and 0.75. Larger a/b (0.85) gives rise to both “standard” ruptures
 190 (constant stress drop cracks), and elastodynamic events decaying as they expand, followed by
 191 slow crack-like ruptures. This pattern results in a period-2 cycle, with the duration of each sub-
 192 cycle consistent with eq. 9, as discussed below.

193 We note that eq. 9 has the same form as the recurrence interval estimated assuming a
 194 constant stress drop circular crack releasing an average slip $v_{pl}T_r = (16/7)\Delta\tau R/\mu'$, but it
 195 is a factor of 7/4 larger. This is consistent with the fact that a fraction of the nominal slip deficit
 196 $v_{pl}T_r$ is released by interseismic creep. There is also a conceptual difference between eq. 9
 197 and the classical argument. The latter is based on assumptions about the rupture occurring at
 198 the end of a cycle: it causes a stress drop $\Delta\tau$ and average slip $v_{pl}T_r$. In contrast, in our deriva-
 199 tion these quantities are related to the interseismic phase: $v_{pl}T_r$ is the slip accumulated in the
 200 velocity strengthening region during a cycle, and *not* necessarily equal to the coseismic slip;
 201 and $\Delta\tau$ is the stress increase between the end of the previous earthquake and steady-state creep
 202 at the loading rate (equal to the stress drop of the previous event). While for period-1 cycles
 203 these are equivalent (since all events have the same $\Delta\tau$), the period-2 cycle for $a/b = 0.85$

204 gives us the opportunity to test these two hypotheses. Every other event is a slow earthquake
 205 and has lower stress drop. According to the classical argument, the longer recurrence inter-
 206 vals are expected to be followed by larger events (size predictable); while according to our ar-
 207 gument, larger quakes should precede the longer recurrence interval, because the large stress
 208 drop will slow down subsequent creep propagation (time predictable). As shown in Fig. 7, the
 209 slow creep events are followed by shorter cycles, consistent with eq. 9; these cycles are about
 210 1.4-1.6 times shorter than the cycles following standard ruptures. The predicted ratio of re-
 211 currence times with $\Delta\tau \sim \log(v_{co}/v_{pl})$, and v_{co} equal to 1 mm/s and 0.1 m/s for slow and
 212 fast ruptures is 1.3.

213 5.2 Onset of lateral ruptures

214 As predicted by a linear stability analysis [Ruina, 1983], a creeping crack with velocity-
 215 weakening friction becomes unstable above a critical dimension (nucleation size), so that lat-
 216 eral ruptures occur on asperities with a radius exceeding some size. Rubin and Ampuero [2005]
 217 estimated a critical dimension for 1D cracks and ageing law friction by treating the rupture
 218 as a constant stress drop crack with a stress intensity factor equal to the toughness determined
 219 from rate-state friction. Assuming steady state friction at seismic slip speeds immediately be-
 220 hind the crack tip, they estimate the maximum half-length for stable propagation to be:

$$L_{\infty} = \frac{1}{\pi} \left(\frac{b}{b-a} \right)^2 L_b \quad (11)$$

For a 2-D crack, we can assume that the rupture starts as a circular, penny-shaped crack within
 the creeping region of the asperity. For this geometry, we have $K_{\Delta\tau,p} = (2/\pi) K_{\Delta\tau,1D}$, where
 the subscripts p (penny) and $1D$ refer to the crack shape shape. The critical radius in 3 di-
 mensions is thus:

$$R_{\infty} = \frac{\pi}{4} \left(\frac{b}{b-a} \right)^2 L_b \quad (12)$$

221 As in the analysis of [Rubin and Ampuero, 2005], this is an upper limit for the nucle-
 222 ation dimension, valid at large slip velocities (e.g. $v \gg v_{pl}$). Since instabilities start within
 223 the creeping annulus in the velocity weakening region (Fig. 2), instabilities can occur when
 224 the creep front has penetrated a distance $L_{pen} = 2R_{\infty}$. With the parameters used in our nu-
 225 merical simulations, $L_{pen} \sim 25L_b = 100$ m. If $R = 2R_{\infty}$ seismic rupture is expected to
 226 start at the center of the asperity, such that this length marks the transition between central and

227 lateral ruptures, which in our simulations occurs at $R \simeq 22L_b = 88$ m, close to the $25L_b$
 228 estimate.

229 At $R < R_\infty = 12.5L_b$, a constant stress drop crack expanding from the center en-
 230 counters the edge of the asperity before reaching v_{dyn} . The slip accelerations observed as the
 231 creep front reaches the center (discussed in section 5.1) have a different geometry and non-
 232 uniform stress drop, and might in principle reach v_{dyn} even on asperities with $R < R_\infty$; while
 233 this does not occur in our simulations, *Chen and Lapusta* [2009] found small events reaching
 234 seismic velocities at $R = 0.93R_\infty$. In our simulations, we find that the transition between
 235 aseismic and seismic slip occurs slightly above $R_\infty = 12.5 L_b$ (between $R = 12.5 L_b$ and
 236 $15.7 L_b$, Fig. 6).

237 To estimate the time to nucleation since the last rupture, we make use of the equation
 238 of motion of the creep front derived in appendix A. Setting $a(t) = R - 2R_\infty$ in eq. 10, and
 239 combining this result with eq. 9, we obtain the nucleation time:

$$T_{nucl} = \begin{cases} R/\dot{r}_c & R < 2R_\infty \\ 4R_\infty (1 - R_\infty/R)/\dot{r}_c & R \geq 2R_\infty \end{cases} \quad (13)$$

240 This is shown by the blue line in Fig. 6, which provides a close fit to the simulated re-
 241 currence times. For $R \gg R_\infty$, $T_{nucl} = 4R_\infty/\dot{r}_c$: the time to nucleation becomes indepen-
 242 dent of R . This is not surprising since this is approaching the 2D limit, when the creep front
 243 propagation is independent of R . However, it would be unphysical for the recurrence inter-
 244 val for full ruptures to be constant above a certain source radius. To understand earthquake
 245 cycles for $R \geq 2R_\infty$, we need to consider the conditions that determine rupture evolution
 246 and arrest, discussed in the following section.

247 **5.3 Rupture propagation and arrest for $R \geq 2R_\infty$**

Ruptures nucleating laterally have to propagate through the locked part of the asperity
 ($r < R - 2R_\infty$). As they propagate towards the center, they encounter lower stresses (since
 the stress imparted by creep decreases with distance from the asperity edge: eq. A.5, fig. B.2).
 Therefore, ruptures may arrest within the locked region and not evolve into full ruptures [as
 previously observed by e.g. *Rice*, 1993; *Lapusta*, 2003; *Wu and Chen*, 2014]; the recurrence
 interval, taken as the time between full ruptures, will be longer than T_{nucl} . We estimate the
 time between full ruptures by requiring that the minimum value of the SIF during rupture prop-
 agation balance K_c (the toughness associated with a crack slipping at coseismic speeds; e.g. *Werner*

and Rubin [2013]). In appendix B we show that in this case Eq. 7 reduces to

$$K_l^* = K_c \quad (14)$$

where K_l^* is the minimum value of the SIF during propagation for a crack loaded by creep since the previous rupture. While an exact calculation of K_l^* requires knowing the shape of the crack as it evolves, dimensional arguments in appendix B lead to:

$$K_l^* = \frac{\mu' v_{pl} t}{\sqrt{R}} \phi, \quad (15)$$

where ϕ is a non-dimensional factor related to the shape of the rupture and its position within the asperity. The minimum time for full ruptures is therefore :

$$T_{full} = \frac{K_c \sqrt{R}}{\phi \mu' v_{pl}}. \quad (16)$$

248 Assuming that the recurrence interval is close to T_{full} , we expect the scaling $T_r \sim \sqrt{R}$. This
 249 estimate of T_{full} ignores the influence of stress perturbations due to prior partial ruptures, which
 250 can be significant, and is therefore approximate. In order to estimate plausible values of T_{full} ,
 251 in Appendix B we calculate ϕ numerically for a simplified rupture history, which gives $\phi =$
 252 0.76. We point out that this value, and hence the minimum radius at which partial ruptures
 253 occur, is an order of magnitude estimate, since it greatly simplifies the shape and evolution
 254 of seismic ruptures: we discuss this issue in more detail below.

We calculate K_c in Appendix B, following Rubin and Ampuero [2005]:

$$K_c = \sqrt{\mu' d_c b \sigma} \log \left(\frac{v_{co} \theta_i}{d_c} \right) \quad (17)$$

255 where θ_i is the state variable just outside the crack tip. Due to healing, this increases with time
 256 since the previous rupture. For the range of recurrence intervals considered, this has an effect
 257 of less than 10% on K_c , and for simplicity we set $\theta_i = 1$ year.

Partial ruptures can occur when $T_{nucl} < T_{full}$. Setting the second of eq. 13 equal to eq. 16, with $\Delta\tau = \tau_{ss}(v_{pl}) - \tau_{ss}(v_{co}) = (b - a)\sigma \log(v_{co}/v_{pl})$, and making use of the expression for fracture energy for the ageing law (eq. A.14), the critical radius for partial ruptures is the solution of

$$\sqrt{\frac{R_\infty}{R}} \left(1 - \frac{R_\infty}{R} \right) = \frac{\sqrt{\pi} \log(v_{co} \theta_i / d_c)}{8 \phi \log(v_{co} / v_{pl})} \quad (18)$$

258 which, for the values of ϕ and θ_i used above, is satisfied by $R = 4.2R_\infty$. We note that eq.18
 259 is a function of the ratio R/R_∞ and numerical constants, with only a weak dependence on
 260 the state variable and slip velocities. The dependence on stress drop and fracture energy (or,

261 equivalently, rate-state parameters and σ) are included in the definition of R_∞ . As for the pre-
 262 vious transitions in rupture style, the ratio R/R_∞ defines the onset of partial ruptures. In the
 263 simulations, we find that the transition occurs between $R = 6R_\infty$ and $R = 8R_\infty$. This dif-
 264 ference is most likely due to the approximations involved in estimating ϕ , as discussed below.

265 **5.4 Ruptures in the $R \gg R_\infty$ regime**

266 To test the criterion for full ruptures expressed by eq. 16, we ran simulations with dif-
 267 ferent parameters in the velocity weakening region ($b - a = 0.01, 0.016$), shown in Fig. 8.
 268 These values are chosen to cover a wide range of asperity dimensions R , while remaining in
 269 the large R/R_∞ regime, and maintaining computational feasibility. The line defining T_{full}
 270 estimated above (eq. 16) separates most partial ruptures from full ruptures, as expected; but
 271 there are some exceptions. In some cases (mostly at $R/R_\infty = 8$, and a single event for $R/R_\infty =$
 272 10), we observe convex ruptures starting with a “horse shoe” shape, which first propagate along
 273 the creeping annulus and then cover the center (triangles in Fig. 8). Not surprisingly, the min-
 274 imum time for full ruptures with ϕ estimated in Appendix B assuming an elliptical rupture (dot-
 275 ted line) fails to capture events with such a different rupture style. The disappearance of these
 276 events at larger R/R_∞ is probably due to this mode of propagation being determined by the
 277 creeping annulus, which becomes increasingly less significant (as a fraction of the asperity)
 278 as $R/R_\infty \rightarrow \infty$. Since all simulations have the same value of b (and hence fracture energy
 279 and K_c), we expect the recurrence interval to follow the scaling \sqrt{R} . On the other hand, the
 280 scaling derived from the classical argument assuming slip to be proportional to $v_{pl}T_r$ predicts
 281 $T_r \sim R\Delta\tau \sim R(b-a)$ (both scalings are shown graphically in Fig. 8). In spite of the scat-
 282 ter in recurrence intervals, the plot suggests that simulations are better explained by the $K_l \geq$
 283 K_c argument. While we chose small a/b values for computational reasons, we note that larger
 284 values of a/b (~ 0.9) are favored by laboratory experiments [Blanpied *et al.*, 1998]. For small
 285 asperities, we observe more complex slip histories for large a/b , and in particular $a/b = 0.85$
 286 (fig. 7), in agreement with previous studies [Rubin and Ampuero, 2005; Noda and Hori, 2014];
 287 it is plausible that larger values of a/b would result in different behavior at large R/R_∞ .

288 In summary, we expect the recurrence interval to scale as $T_r = T_{nucl} \sim R$ on small
 289 asperities ($R < 2R_\infty$), and approximately as $T_r = T_{full} \sim \sqrt{R}$ on larger asperities ($R \gtrsim$
 290 $4.2R_\infty$), and with an intermediate exponent between the two (when $T_r \sim T_{nucl}$, but T_{nucl}
 291 scales sub-linearly with R). This is in broad agreement with numerical simulations (Fig. 6).

6 Stress drops and scaling between T_r and M_0

Crack models allow us to derive scaling relations between recurrence interval and source dimension. To understand the scaling with seismic moment ($M_0 \sim \mu \Delta \tau R^3$), we need to consider how stress drops scale with source radius. Fig. 9b shows how the seismic moment scales with R in the simulations, obtained from eq.1 with M_0 given by integrating slip over the area during time steps with $v \geq v_{dyn}$ anywhere on the asperity. For the 5 smallest faults, an increase in stress drop with fault dimension is visible: this is due to a fraction of the seismic moment being released during the nucleation phase. Slip profiles during the seismic phase are well approximated by an elliptical crack with constant stress drop until the crack reaches the edge of the asperity, and by a circular, penny-shaped crack at the end of the earthquake. This is consistent with a constant and spatially uniform stress drop during rupture growth, and the same stress drop for earthquakes of different size as shown in Fig. 9. However, fig. 9a shows that some of the slip is accumulated aseismically and thus does not contribute to the coseismic moment, defined as the moment released when $v \geq v_{dyn}$.

As the crack expands, the slip velocity increases. The crack starts slipping at seismic velocities once it reaches a finite size (R_∞). We can then calculate the moment released during the nucleation phase from the moment of a penny-shaped crack of radius R_∞ . The coseismic moment is then given by

$$M_0 = M_{0tot} - M_{aseis} = \frac{16}{7} \Delta \tau (R^3 - R_\infty^3) \quad (19)$$

where the first term is the total moment released from the beginning of nucleation phase to the end of the earthquake. The ratio between seismic and total moment is $1 - (R_\infty/R)^3$ and it quickly approaches 1 (for example, almost 90% of the moment is released coseismically for $R = 2R_\infty$, which corresponds to the transition between central and lateral ruptures). This indicates that the variation in stress drops is only expected to occur over a limited range of fault dimensions.

From the simulations, we find that crack reaches $v = v_{dyn}$ when the semi-major and minor axes reach 55 m, 42 m respectively, in the inplane and antiplane directions, close to our estimate of R_∞ (50 m). As expected, this dimension is approximately independent of asperity dimension R (Fig. 9a). We estimate the total moment M_{0tot} directly from the slip profile: $M_{0tot} = \mu \pi S R^2 / 2$, where S is the slip at the center of the asperity. We find that the scaling of M_{0tot} from the simulations is consistent with self-similarity, as expected from the fact that the slip profiles in Fig. 9(a) have roughly the same shape. Furthermore, the scaling of M_0

319 with R is in agreement with eq. 19. For the smallest fault ($R \sim 1.3R_\infty$), the stress drop es-
 320 timated from M_0 is about 50% smaller than the stress drop estimated from M_{0tot} .

321 Finally, we are in a position to combine the scaling of seismic moment with R and the
 322 dependence of T_{full} and T_{nucl} (eq. 16 and 13). This is shown in Fig. 10. While some slight
 323 variations in the exponent are seen, we find that in the range $R_\infty < R \lesssim 4.2R_\infty$, the pre-
 324 dicted trend is close to $T_r \sim M_0^{1/6}$. For $R \gtrsim 4.3R_\infty$, we expect $T_r \sim M_0^{1/6}$ scaling from
 325 constant stress drop and $T_{full} \sim \sqrt{R}$. This is the central result of the paper.

326 6.1 Coseismic and interseismic slip budget

327 Figs. 11 and 12 show the contribution of seismic and aseismic slip on asperities with
 328 different R/R_∞ . Aseismic stress release occurs in various phases of the seismic cycle: (1) dur-
 329 ing the interseismic period, as creep fronts propagate inwards and parts of the asperities slip
 330 at a speed of the order of v_{pl} ; (2) during aseismic slip episodes such as those shown in Fig. 2;
 331 (3) during the acceleration and deceleration phase of an earthquake. The fraction of aseismic
 332 slip in phase (3) depends on the definition of ‘‘coseismic’’ slip velocity. The condition that the
 333 long-term slip rate on the asperity matches the loading rate can be expressed as follows:

$$S_{tot} = v_{pl}T_r = S_{seis} + S_{creep} + S_{nucl} + S_{post} \quad (20)$$

In Appendix C we derive analytical expressions for S_{creep} and S_{nucl} as a function of R/R_∞ . The derivation of S_{nucl} is essentially equivalent to eq. 19, and it is based on the observation that slip shown by the dotted elliptical profiles in Fig. 9 accumulates between the time when the creep front reaches the center and the onset of the seismic phase (blue and yellow lines in the slip profiles in Fig. 1); on the other hand, S_{creep} approximates the slip due to creeping at $v \sim v_{pl}$ (black lines in Fig. 1). Simulations do not exhibit significant postseismic slip within the velocity weakening asperity (Figs. 11, 12), consistent with results from spring slider simulations [Rubin and Ampuero, 2005; Segall, 2010]. We therefore neglect this process as well as the contribution of transient aseismic slip episodes and partial ruptures for $R \gtrsim 4.3R_\infty$. Because of the latter assumption, these results are strictly valid only for $R \lesssim 4.3R_\infty$. Fig. 13a shows predicted S_{tot} , S_{creep} and S_{nucl} as a function of R/R_∞ . As expected, S_{tot} has the same trend as T_r (Fig. 6). The slip from interseismic creep is also proportional to T_{nucl} for $R < 2R_\infty$ (asperities on which the creep front reaches the center); in Appendix C we show that $S_{creep}/S_{tot} = 0.25$. For larger values of R , interseismic creep is confined

to part of the asperity $r > R - 2R_\infty$, and its contribution decreases with R . Finally, the fraction of slip during the nucleation phase decreases monotonically with R . Combining these results we estimate the ratio of seismic to total slip as

$$\frac{S_{seis}}{S_{tot}} = 1 - \frac{S_{as}}{S_{tot}} = 1 - \frac{S_{creep} + S_{nucl}}{S_{tot}} \quad (21)$$

334 shown in Fig. 13b. The ratio of seismic to aseismic slip derived from simple crack models pro-
335 vides a reasonable fit to the trend the simulations.

336 7 Discussion

337 Based on energy balance arguments, and the scaling of stress intensity factors with as-
338 perity dimension, we identified the following regimes:

- 339 • $R < R_\infty$: asperities are aseismic.
- 340 • $R_\infty < R < 2 R_\infty$, creep completely erodes the asperity and seismic rupture nucle-
341 ate from the center. The recurrence interval scales as $T_r \sim R$. Stress drops increase
342 weakly with R .
- 343 • $2 R_\infty < R \lesssim 4.3 R_\infty$: creep partially erodes the asperity before ruptures nucleate.
344 When this occurs, the elastic energy accumulated from creep is sufficient for the rup-
345 ture to propagate across the entire locked region, so that every nucleation results in a
346 full rupture. The recurrence interval scales with $T_r \sim \sqrt{R}$.
- 347 • $R \gtrsim 4.3 R_\infty$: the energy required for a rupture to propagate through the locked re-
348 gion exceeds the energy required for nucleation, and partial ruptures occur. The recur-
349 rence interval of full ruptures is expected to scale as $T_r \sim \sqrt{R}$.

350 These results are broadly in agreement with *Chen and Lapusta* [2009], who found sim-
351 ilar transition when increasing R with constant rate-state parameters, and *Kato* [2014]. It is
352 important to note that the transitions depend on the ratio R/R_∞ , and not on the earthquake
353 moment: the x-axis in Fig. 3 and 10 would take different values for different rate-state param-
354 eters or normal stress. The onset of partial ruptures at a sufficiently large value of R/R_∞ is
355 essentially based on a comparison between the nucleation length and the overall asperity di-
356 mension. The fracture energy argument leading to $R_{nucl} = R_\infty$, proposed by *Rubin and Am-
357 puero* [2005] and confirmed for circular asperities by *Noda and Hori* [2014], only applies for
358 sufficiently large values of a/b (> 0.37). For smaller a/b , nucleation occurs on a length scale
359 of $\sim 1.7L_b$ [*Dieterich*, 1992; *Noda and Hori*, 2014]: therefore in this case we expect all tran-

360 sitions to occur at values of R/R_∞ different from those predicted here. For example, this is
 361 consistent with the observation that $R/R_\infty = 8$ produces partial ruptures with $a/b = 0.5$,
 362 0.75 , but not with $a/b = 0.2$ (Fig. 8). For $a/b = 0.2$, the nucleation radius ($R_{nucl} = 1.7L_b$)
 363 is larger than R_∞ by a factor of 1.4; the ratio of asperity radius to nucleation radius is there-
 364 fore lower ($R/R_{nucl} = 5.7$). As expected, this asperity exhibits a behavior similar to the one
 365 with $a/b = 0.75$ and $R/R_\infty = 6$ (the second largest asperity in Fig. 6), which does not
 366 have partial ruptures. But since such low values of a/b are not supported by lab experiments [e.g.
 367 *Blanpied et al.*, 1998], in realistic cases we expect the ratio R/R_∞ to determine rupture be-
 368 havior.

369 Interestingly, we find that the scaling between seismic moment and recurrence interval
 370 arises from different physical reasons depending on R . For small asperities, the recurrence in-
 371 terval scales linearly with dimension; in this range of R , it is the increase of $\Delta\sigma$ with R that
 372 gives rise to $T_r \sim M_0^{1/6}$ scaling. The non-constant stress drop as R approaches the nucle-
 373 ation length is not surprising: crack models which predict constant $\Delta\tau$ assume a point source
 374 at $t = 0$, while the existence of a finite nucleation dimension breaks self-similarity as R ap-
 375 proaches R_∞ . For asperities with $R > 2R_\infty$, on the other hand, the relationship between
 376 T_r and M_0 is dominated by the $T_r \sim \sqrt{R}$ scaling, which originates from the dependence
 377 of the stress intensity factor on asperity dimension. In other words, we recover the observed
 378 scaling by considering seismic ruptures as releasing accumulated elastic energy rather than stress.

379 A simplification in our crack models is the neglect of inertia when balancing the stress
 380 intensity factor and fracture toughness. While this assumption is valid for modeling creep prop-
 381 agation (and hence T_{nucl}), when applied to seismic ruptures it may lead to an underestima-
 382 tion of T_{full} . An assumption behind our analysis is that the distribution of M_0 is dominated
 383 by variations in asperity dimension R , while spatial variations in physical properties play a
 384 secondary role. In reality, frictional parameters and normal stress are not necessarily uniform,
 385 and R_∞ can vary spatially. Assuming that such variations are independent of scale, this will
 386 generate scatter around the trend modeled here (since we found $T_r \sim M_0^{1/6}$ across a wide
 387 range of R/R_∞) but not affect the trend itself; since the results derived here imply that each
 388 “family” of asperities with given physical properties would fall on a $T_r \sim M_0^{1/6}$ line with
 389 a different proportionality constant. Additional heterogeneity with each asperity, due to fault
 390 roughness or variations in frictional and elastic properties, will also lead to more scatter in source
 391 properties and scaling. With this caveats in mind, below we discuss possible seismological ob-
 392 servations predicted by our models.

393

7.1 Relating observed recurrence intervals to $\Delta\tau$ and R_∞

The analytical expressions for T_{nucl} , T_{full} and M_0 (eq. 13, 16, 19; Fig. 10) allow us to estimate fault properties from the relationship between seismic moment and recurrence interval observed in nature. *Nadeau and Johnson* [1998] observed the relationship

$$\log_{10}(T_r) = 0.17 \log_{10}(M_0) + 6.0 \quad (22)$$

394

with T_r is the recurrence interval in seconds and M_0 the seismic moment in Nm. *Chen et al.*

395

[2007] found that the same expression applies to repeating sequences in Taiwan and Japan,

396

after rescaling the recurrence interval by the background creep rates in each location.

In the regime $R \geq 4.3 R_\infty$, we obtain this scaling from M_0 and T_{full} (eqs. 1 and 16): the constant of proportionality between T_r and $M_0^{1/6}$ is a function of fracture toughness K_c . On the other hand, for $R < 4.3$ the recurrence interval T_{nucl} as a function of M_0 is given by eq. 13 and 19, which are functions of stress drop and nucleation length. We can reconcile the two by noting the relationship between K_c (eq. 17), R_∞ (eq. 12), and $\Delta\tau = \tau_{ss}(v_{pl}) - \tau_{ss}(v_{co})$, with τ_{ss} from eq. 4:

$$\frac{K_c}{\Delta\tau} = \frac{\sqrt{d_c b \sigma \mu'} \log(v_{co} \theta_i / d_c)}{(b-a)\sigma \log(v_{co}/v_{pl})} \approx 1.3 \frac{\sqrt{d_c b \sigma \mu'}}{(b-a)\sigma} = 2.6 \sqrt{R_\infty / \pi} \quad (23)$$

397

where we estimated the logarithmic terms as in section 5.3. Combining this expression with

398

eq. 16 and taking the ratio between T_{full} and $M_0^{1/6}$ (with eq. 1 relating M_0 to R), we get

$$\frac{T_{full}}{M_0^{1/6}} = \frac{2.6(7/16)^{1/6} \sqrt{R_\infty / \pi} \Delta\tau^{5/6}}{\phi \mu' v_{pl}} \approx \frac{1.6 \sqrt{R_\infty} \Delta\tau^{5/6}}{\mu' v_{pl}} \quad (24)$$

399

where we used $\phi = 0.76$, as before.

For $R < 4.3 R_\infty$, the scaling is given by $T_{nucl}(R)$ and $M_0(R)$ (eq. 13 and 19). Fig. 10 shows that these expression yield a scaling close to $T_r \sim M_0^{1/6}$, but with some slight variations. To facilitate comparison with eq. 22, we take the ratio between T_r and $M_0^{1/6}$:

$$\frac{T_{nucl}}{M_0^{1/6}} = \frac{\sqrt{R_\infty}}{r_c \Delta\tau^{1/6}} f(R/R_\infty) \quad (25)$$

400

with

$$f(x) = \begin{cases} \left(\frac{7}{16}\right)^{1/6} \frac{x}{(x^3 - 1)^{1/6}} & R < 2R_\infty \\ \left(\frac{7}{16}\right)^{1/6} \frac{4(1 - 1/x)}{(x^3 - 1)^{1/6}} & R \geq 2R_\infty. \end{cases} \quad (26)$$

The function $f(R/R_\infty)$ quantifies the variations of T_{nucl} around a line of constant $M_0^{1/6}$ (see Fig. 10). It is singular at $R = R_\infty$ (since the stress drop, and seismic moment, tend to 0);

for R/R_∞ between 1.1 and 4.3, it ranges between 1.1 and 1.35, with an average value of 1.28.

Therefore we take $f(R/R_\infty) \approx 1.3$ and recalling that $\dot{r}_c = \pi\mu'v_{pl}/4\Delta\tau$, we can write

$$\frac{T_{nucl}}{M_0^{1/6}} \approx \frac{1.6\sqrt{R_\infty}\Delta\tau^{5/6}}{\mu'v_{pl}} \quad (27)$$

Note that eq. 27 and 24 are the same, as expected from visual comparison of T_{nucl} (for $R < 4.3 R_\infty$) and T_{full} in fig. 10. We are now in a position to relate the theoretical scalings with the observations. Setting eq. 27 equal to eq. 22, we find the constant of proportionality between $M_0^{1/6}$ and T_r :

$$\frac{T_r}{M_0^{1/6}} = \frac{1.6\sqrt{R_\infty}\Delta\tau^{5/6}}{\mu'v_{pl}} \approx 10^6 \quad (28)$$

401 *Chen and Lapusta* [2009] found that numerical simulations with $v_{pl} = 23\text{mm/yr}$ (the
 402 creep rate inferred by *Nadeau and Johnson* [1998] at Parkfield) produced shorter recurrence
 403 intervals than observed, and suggested that the long term creep rate must be lower (4.5mm/yr).
 404 Eq. 28 shows that the recurrence rate is determined by the creep rate, the nucleation length
 405 and the stress drop. Combinations of these quantities which can explain the observed scaling
 406 are shown in Fig. 14: each line indicates the background creep velocity required to explain
 407 the observed recurrence interval, as a function of $\Delta\tau$ and for a given value of R_∞ . In spite
 408 of the approximations in eq. 28, we recover the result from the numerical simulations by *Chen*
 409 *and Lapusta* [2009]: their value of stress drop and R_∞ (~ 4 MPa and ~ 83 m respectively)
 410 require $v_{pl} = 4.5$ mm/yr to explain the observed recurrence interval. They also noted that
 411 increasing d_c results in a longer recurrence interval, as can be seen in Fig. 14; however, the
 412 nucleation length in this case becomes too large to explain the small magnitudes found at Park-
 413 field (several events close to $M_w \sim 0$, *Nadeau and Johnson* [1998]).

414 It is plausible that local the creep rate near the repeaters may be lower or higher than
 415 23 mm/yr: as *Nadeau and Johnson* [1998] note, the geodetic inversion by *Harris and Segall*
 416 [1987], on which this value is based, shows variations between 4 mm/yr and 35 mm/yr near
 417 the repeater sequences. However, *Chen et al.* [2007] noted that sequences of repeating events
 418 in Taiwan and Japan follow the same scaling after renormalizing the recurrence interval by
 419 inferred creep rate in each region, and this implies that the creep rate would have been over-
 420 estimated by the same factor in these locations. In alternative, a nucleation length of 10–100
 421 m and a creep rate of about 23 mm/yr can explain the observed T_r if stress drops are between
 422 30–100 MPa, somewhat on the higher end of seismological values estimated for Parkfield
 423 repeaters [*Abercrombie*, 2014; *Imanishi and Ellsworth*, 2006] and in Japan [*Uchida et al.*, 2007],
 424 shown in Fig. 14. A smaller nucleation length (~ 1 m) may be more realistic considering that

425 even smaller events have been observed at Parkfield ($M_w \lesssim -0.5$, e.g. *Nadeau and Johnson*
 426 *[1998]*; W. Ellsworth, private communication, 2018); this requires either very high stress
 427 drops (~ 400 MPa for $v_{pl} = 23$ mm/yr), or a much lower creep rate or shear modulus; or
 428 a combination of the these. The large uncertainties in estimated stress drops [see for exam-
 429 ple *Kaneko and Shearer, 2014*, and section 7.2] and in the local creep rate make it challeng-
 430 ing to determine which of these factors is dominant. Based on the available stress drops mea-
 431 surements, our preferred interpretation is that stress drops are in the 10–100 MPa range, and
 432 local creep rates are probably lower than 23 mm/yr.

Eq. 28 provides a physical interpretation for the scaling first observed by *Nadeau and Johnson [1998]*, eq. 22. A more commonly used form of this expression relates the interseismic slip $v_{pl}T_r$ to the seismic moment, and can be obtained multiplying both sides of Eq. 28 by v_{pl} . Based on the observations of *Nadeau and Johnson [1998]* at Parkfield, several studies have used small repeaters as creepmeters [e.g. *Uchida et al., 2003, 2006; Turner et al., 2015; Materna et al., 2018*]. Our expression shows that estimating creep rates from the Parkfield observations is appropriate, as long as the nucleation length and stress drops are comparable to Parkfield. Since $\sqrt{R_\infty}$ scales inversely with stress drop (eq. 23), the dependence of T_r on $\Delta\tau$ is weak; we can see this from eq. 16, or by combining eq. 23 and 28:

$$\frac{T_r}{M_0^{1/6}} = \frac{2\sqrt{d_c b \sigma \mu'}}{\pi \mu' v_{pl} \Delta\tau^{1/6}} \quad (29)$$

433 Variations in normal stress, μ' , d_c or b , on the other hand, affect the recurrence interval more
 434 strongly. Therefore, the universal scaling observed by *Chen et al. [2007]* imply comparable
 435 fracture energy in the regions considered.

436 7.2 Observations near the nucleation dimension

437 The existence of a finite nucleation dimension (R_∞) introduces a break in self similar-
 438 ity. While the value of R_∞ estimated here is specific to rate-state friction with certain param-
 439 eters, we expect this result to be general: since the stiffness of a constant stress drop crack is
 440 inversely proportional to its size, slip on cracks below a critical dimension is aseismic [e.g.
 441 *Ruina, 1983*].

442 Could this variation in stress drop be observed in nature? The main difference between
 443 a numerical simulation and real earthquakes is that with simulations we know the asperity di-
 444 mension. Therefore, when estimating stress drops, the larger fraction of slip released aseis-
 445 mically on smaller asperities leads to lower stress drops. However, the existence of a finite nu-
 446 cleation dimension also shortens the distance a rupture propagates before reaching the edge

447 of the asperity. Asperity dimension is commonly estimated from the rupture duration, inferred
 448 from the corner frequency and assuming an expanding circular crack with constant rupture ve-
 449 locity [Madariaga, 1977; Sato and Hirasawa, 1973; Kaneko and Shearer, 2015]. For a rup-
 450 ture starting at $r = R_\infty$, the rupture duration will be shorter: in our simulations, it is pro-
 451 portional to $R - R_\infty$. This may lead to underestimation of the asperity dimension as $R \rightarrow$
 452 R_∞ , and overestimation of the stress drops. To further complicate matters, the rupture veloc-
 453 ity is not constant during this phase (since the crack is still accelerating). Therefore, smaller
 454 asperities have lower average rupture velocity, which may partially counteract the previous ef-
 455 fect. These results indicate that assuming a circular source expanding at constant velocity may
 456 lead to large biases in the estimation of source properties at dimensions near R_∞ . We point
 457 out that the definition of “earthquake” used here (based on a velocity threshold) probably does
 458 not accurately reflect the way seismic ruptures are recorded, making it difficult to directly trans-
 459 late our results into observable variations in source properties. In fact, a similar study by *Kato*
 460 [2012b] found constant stress drops for ruptures nucleating at the center, the discrepancy most
 461 likely explained by the use of a lower velocity threshold (0.01 m/s), which resulted in part of
 462 the nucleation phase (as defined in the present study) being included in the earthquake. Fi-
 463 nally, we note that the final phase of the inward creep propagation for events that nucleate near
 464 the asperity center can result in peak velocities close to v_{dyn} , described in section 5.1. In our
 465 pseudo-dynamic simulations, these events occurred minutes or hours before the main shock,
 466 and were significantly smaller; they do however indicate that nucleation due to the convergence
 467 of a creep front may result in a more complex source-time function than a simple constant stress
 468 drop crack.

469 7.3 Transition between central and lateral ruptures

470 Circular sources propagating radially from the center are often used to infer source prop-
 471 erties for small to moderate earthquakes. However, our results suggest that central ruptures only
 472 take place on asperities within a narrow range of dimensions ($R_\infty < R < 2R_\infty$), and should
 473 therefore be quite rare for repeating earthquakes in nature.

474 Studies of rupture directivity for moderate to small events (down to about $M3.0$) indi-
 475 cate a prevalence of unilateral ruptures, with no variation with magnitude [Boatwright, 2007;
 476 *Abercrombie et al.*, 2017; *Calderoni et al.*, 2015]. A transition to central ruptures may occur
 477 at smaller magnitudes, for which estimating rupture directivity (or lack thereof) is particularly
 478 challenging.

7.4 Observations at large R/R_∞

Finally, we estimated the minimum asperity radius that can host partial ruptures. While the exact dimension of the transition depends on the details of the asperity shape and assumptions in the derivation, the existence of such transition can be understood intuitively. Loading from the boundary of an asperity creates stress gradients within it, with lower stresses further away from the loading point. Stress increases everywhere with time, until an event can nucleate at the edge. If the asperity is large, the rupture will have to penetrate through a more extended region of lower stress, where it is more likely to arrest. This can also apply to other fault geometries: for example, *Rice* [1993], *Werner and Rubin* [2013] and *Herrendorfer et al.* [2015] found a similar transition in 2-D models of faults loaded by creep below the seismogenic zone, and *Wu and Chen* [2014] observed this transition in 2-D faults loaded from both ends. Similar concepts have been invoked to explain rupture arrest in laboratory experiments [*Kammer et al.*, 2015]. *Kato* [2014] also observed a similar transition in simulations at constant R and variable d_c , with low d_c resulting in partial ruptures. Moreover, he noted that the recurrence interval scales as $\sqrt{d_c}$, in agreement with the prediction from T_{full} in eq. B.5 (since $K_c \sim \sqrt{d_c}$, as can be seen from eq. 8 and eq. A.14).

We demonstrated that the recurrence interval of full ruptures for $R \gtrsim 4.2R_\infty$ is expected to scale as $T_r \sim \sqrt{R}$, leading to the moment scaling observed in nature for repeating events: it is likely that most of the observed repeaters are in this regime. An interesting question is how the occurrence of partial ruptures may affect the degree of periodicity of the system. Partial ruptures introduce variability in the stress field, not considered in our derivation: for example, a rupture may arrest in a low stress region caused by a previous rupture [*Lapusta*, 2003], or be promoted by the stress concentrations outside its perimeter. These factors may affect not only the recurrence interval of full ruptures, but also their slip evolution and observed waveforms, practically determining an upper bound to the characteristic behavior that defines a repeater. We note that the simulation with partial ruptures presents more variability in recurrence interval than those without (Fig. 4); however, due to computational costs this simulation only produces a small number of full ruptures (3), and we cannot draw strong conclusions. Further studies are needed to verify whether asperities above a certain dimension lose the periodicity and characteristic behavior. Some indications of periodicity at large R/R_∞ can be inferred from the observed magnitude of repeaters, that can be as large as $M4.9 - 5.0$ [*Chen et al.*, 2009; *Uchida et al.*, 2012]. Combined with the observation that most events above $M3.0$ are unilateral, and therefore in the regime where $R > 2R_\infty$, this suggests that asperities as

512 large as $20R_\infty$ can have characteristic, quasi-periodic behavior. An alternative plausible ex-
 513 planation for this magnitude range may be regional variation in R_∞ . However, more direct
 514 evidence comes from the observation of multiple families of repeaters with overlapping rup-
 515 ture areas [*Uchida et al.*, 2007]: the $M4.9$ Kamaishi (Japan) repeater experiences interseismic
 516 partial ruptures, mostly located near its edge (as expected from the crack models presented here).
 517 Given that most of these partial ruptures are between $2 < M < 3$, the Kamaishi repeater
 518 appears to be an example of a periodic earthquake many times larger than R_∞ .

519 **7.5 Slip budget**

520 *Chen and Lapusta* [2009] explained the scaling of T_r for small R/R_∞ by the increase
 521 of seismic to aseismic slip ratio with R , as seen in Fig. 13; however, direct measurements of
 522 the slip partitioning at such small magnitudes have proven challenging. Using borehole strain-
 523 meter records of small events on the San Andreas fault, *Hawthorne et al.* [2016] observed that
 524 the fraction of postseismic slip doesn't vary significantly as a function of magnitude (note that
 525 these observations could not determine whether slip occurred within or outside of the asper-
 526 ity). Based on our models, we expect aseismic slip on the asperity to occur mainly during the
 527 interseismic and the nucleation phase rather than postseismically. The propagation of the creep
 528 front on a circular fault is such that the creeping area grows approximately linearly with time
 529 (it would be exactly linear for the approximated equation of motion given by eq. 10); for a
 530 constant slip velocity behind the creep front, we thus expect a constant acceleration in mo-
 531 ment. The total moment released by this process is not more than about a quarter of the to-
 532 tal moment. The fractional contribution from the nucleation phase, on the other hand, can be
 533 arbitrarily large (Fig. 13).

534 **8 Conclusions**

535 We developed crack models of circular asperities embedded in a creeping fault, and found
 536 that they successfully reproduce the observed scaling between the recurrence interval and seis-
 537 mic moment: $T_r \sim M_0^{1/6}$. The temporal evolution of the creep front eroding an asperity is
 538 well fit by crack models, allowing us to quantify the contribution from aseismic slip during
 539 different phases of the seismic cycle.

540 Our models make specific prediction on the seismic behavior of asperities as a function
 541 of their dimension with respect to the nucleation radius R_∞ . These findings are strictly valid
 542 for $0.3 < a/b < 0.75$: in this range, simulations with the same ratio R/R_∞ exhibit the same

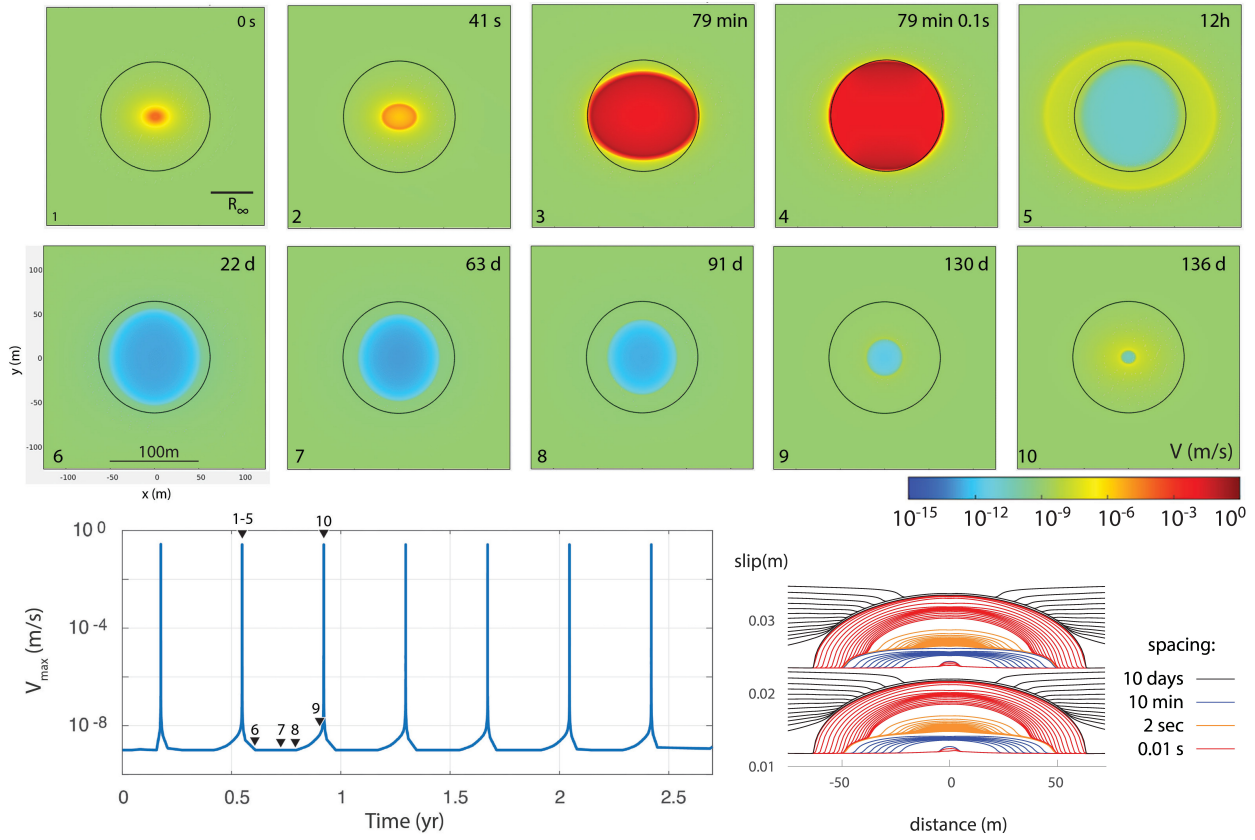
543 behavior. For smaller a/b , R_∞ should be replaced by $1.7L_b$, a better estimate of the nucle-
 544 ation half-length; while for larger a/b , we observe similar scalings, but more variability in rup-
 545 ture style and recurrence interval between cycles. We identify a range of asperities over which
 546 ruptures nucleate from the center ($R_\infty < R < 2R_\infty$). Even though source models for events
 547 below M_5 often assume central ruptures [e.g. *Boatwright, 2007*], we expect this behavior to
 548 be relatively rare due to the narrow range of R/R_∞ that exhibit this rupture style. We also
 549 note that the existence of a finite nucleation size introduces a break in self-similarity, which
 550 results in a decrease of stress drop with decreasing R . This effect leads to the $T_r \sim M_0^{1/6}$
 551 scaling for small asperities.

552 For larger asperities, the same scaling is not due to variations in stress drop or to aseis-
 553 mic slip but to the relationship between stress intensity factor and radius. In particular, we find
 554 that an energy balance argument predicts that full ruptures are possible at $T_{full} \sim \sqrt{R}$, and
 555 hence $T_r \sim M_0^{1/6}$. According to our analysis, this criterion explains the recurrence interval
 556 for asperities above $\sim 4.3R_\infty$. We discuss observational evidence suggesting that the largest
 557 observed repeater (the $M_{4.9}$ Kamaishi, Japan repeater) falls into this regime.

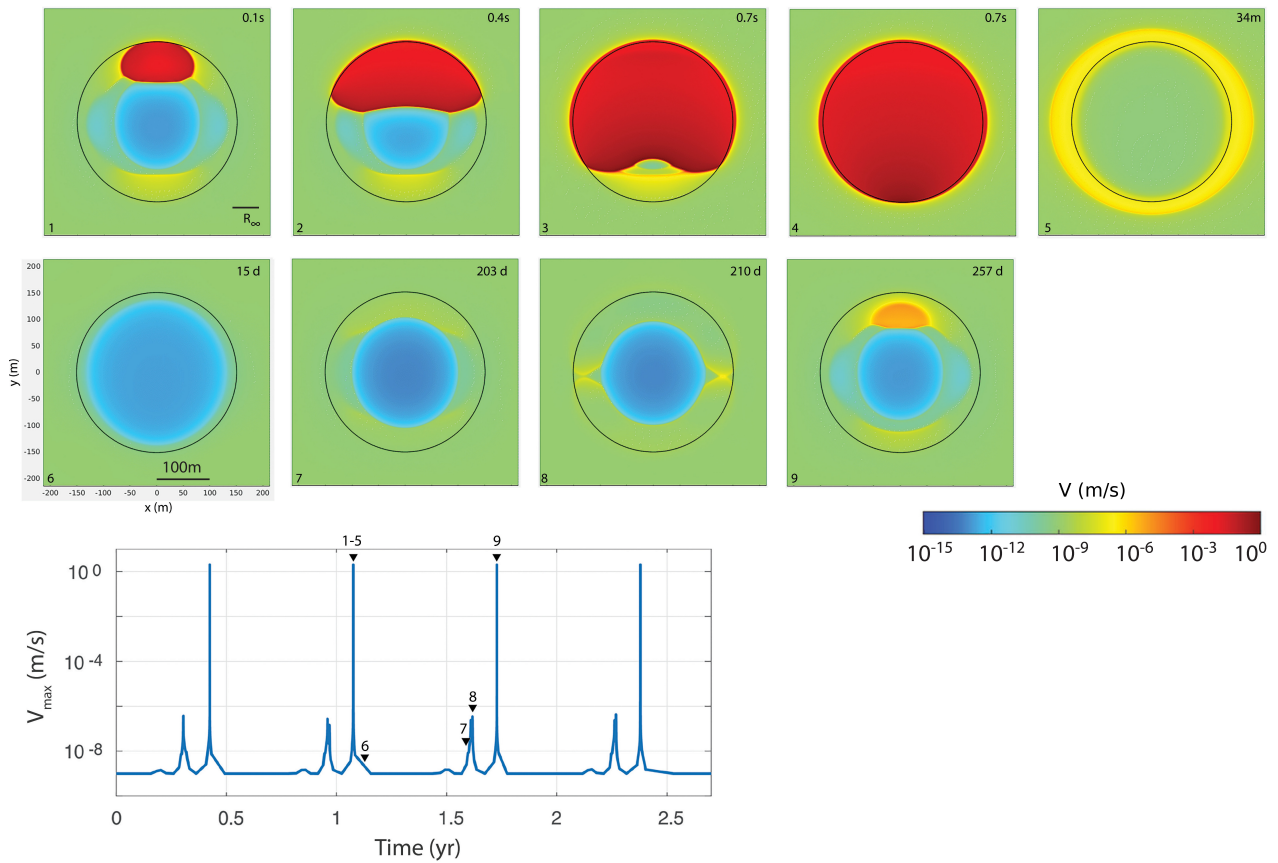
558 We show that the scaling across all regimes is be approximated by: $T_r = \frac{1.6\sqrt{R_\infty}\Delta\tau^{5/6}}{\mu'v_{pl}}M_0^{1/6}$.
 559 The dependence of this expression on the creep rate validates the use of small repeating earth-
 560 quakes as creepmeters, but also highlights the role of fault properties which can affect the re-
 561 currence interval measured on different faults.

562 Acknowledgements

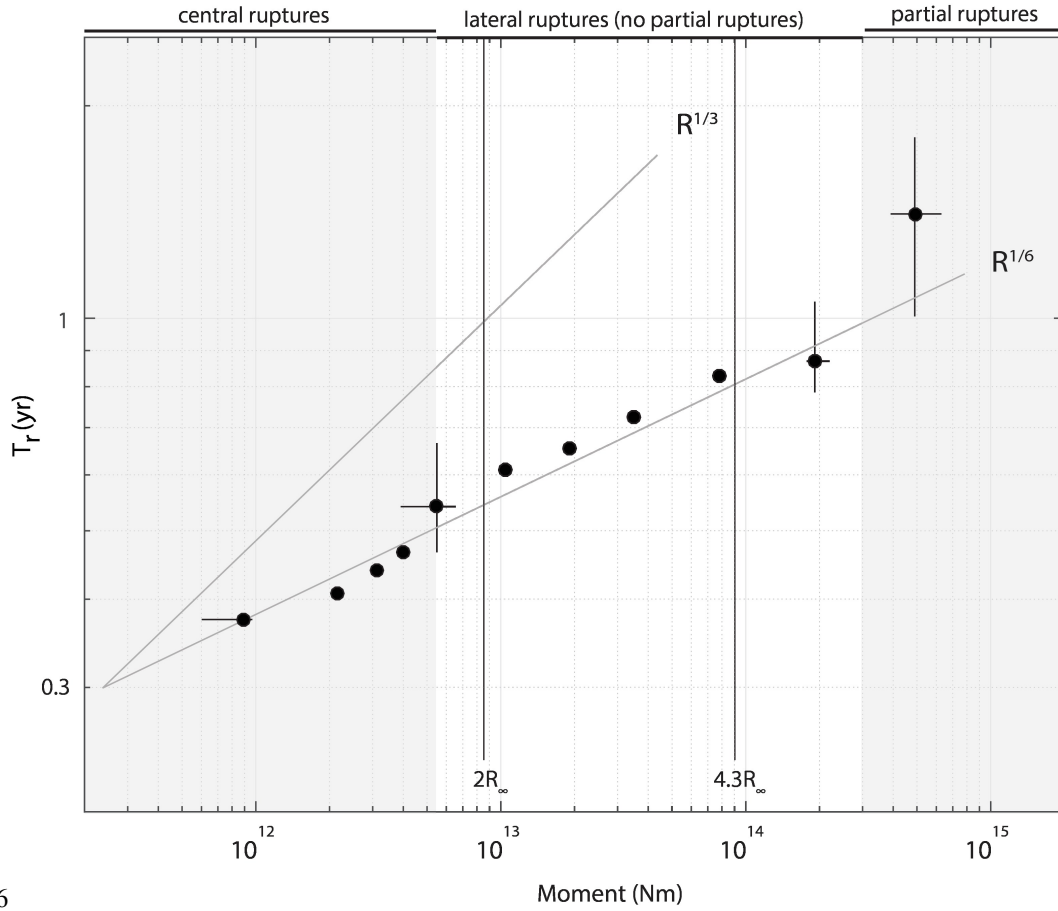
563 We are grateful to Allan Rubin, Sylvain Barbot, and the associate editor for thoughtful
 564 reviews that significantly improved the manuscript. C.C. was supported by the German Aca-
 565 demic Exchange Service (DAAD) with funds from the German Federal Ministry of Educa-
 566 tion and Research (BMBF) and the People Programme (Marie Curie Actions) of the European
 567 Union's Seventh Framework Programme (FP7/2007-2013) under REA grant agreement no. 605728,
 568 and NSF award no. 1620496. No new data was used in this study.



569 **Figure 1.** Top: full rupture on a fault of size $R = 16L_b$ ($1.3R_\infty$). Color is slip speed; slip is in the x direc-
 570 tion. The time since the arrival of the creep front at $r = 0$ is indicated; notice the acceleration in panels 1,2
 571 preceding the main event. Bottom left: maximum slip velocity in the VW region vs. time, showing that this
 572 fault experiences periodic seismic ruptures. Numbers refer to the snapshots above. Bottom right: slip history
 573 over 2 cycles. Red lines indicate the seismic phase ($v > v_{dyn}$); blue and orange lines indicate slip between
 574 the arrival of the creep front and the onset of the seismic phase; black lines indicate interseismic slip.

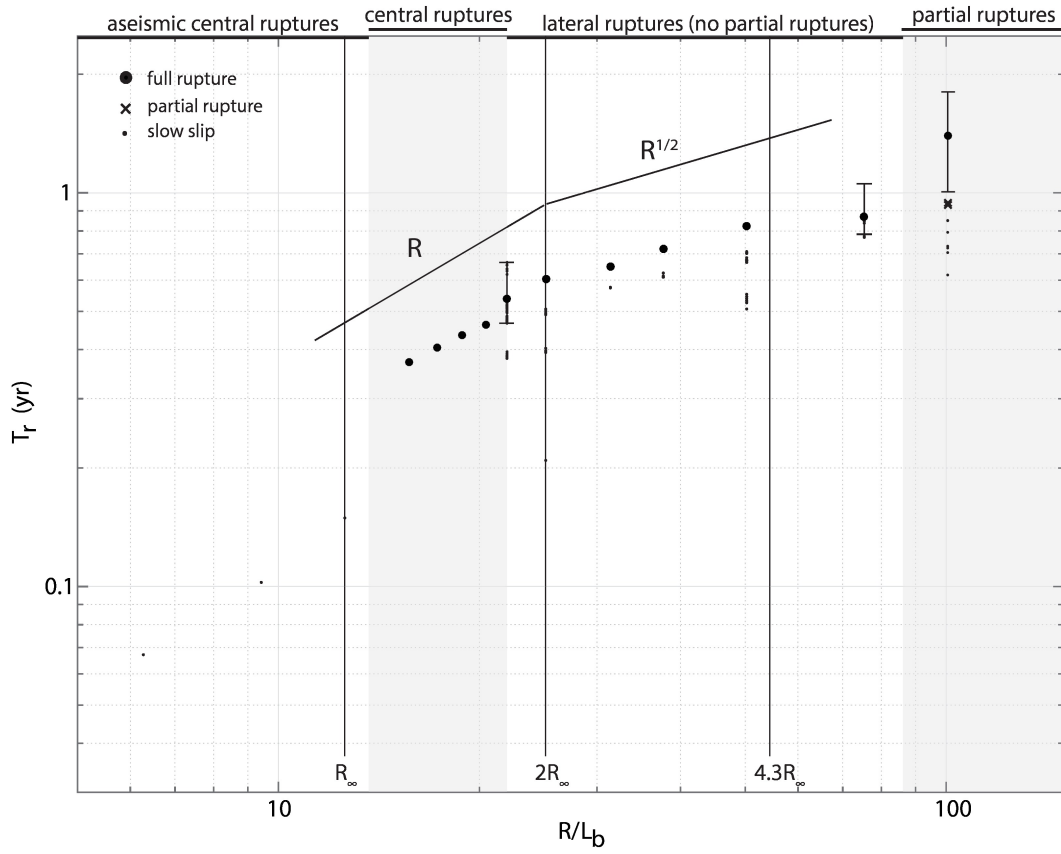


575 **Figure 2.** Example of a seismic cycle on a fault with $R = 38L_b (3R_\infty)$. Color is slip speed. Top: seismic
 576 event (panels 1-4) and afterslip (5). Inward propagation of a creep front, and a slip acceleration that does not
 577 reach seismic velocity (8). The time from the onset of the earthquake is indicated. Bottom: maximum slip
 578 velocity in the VW region vs. time, showing seismic and aseismic slip episodes. Numbers refer to the panels
 579 above.

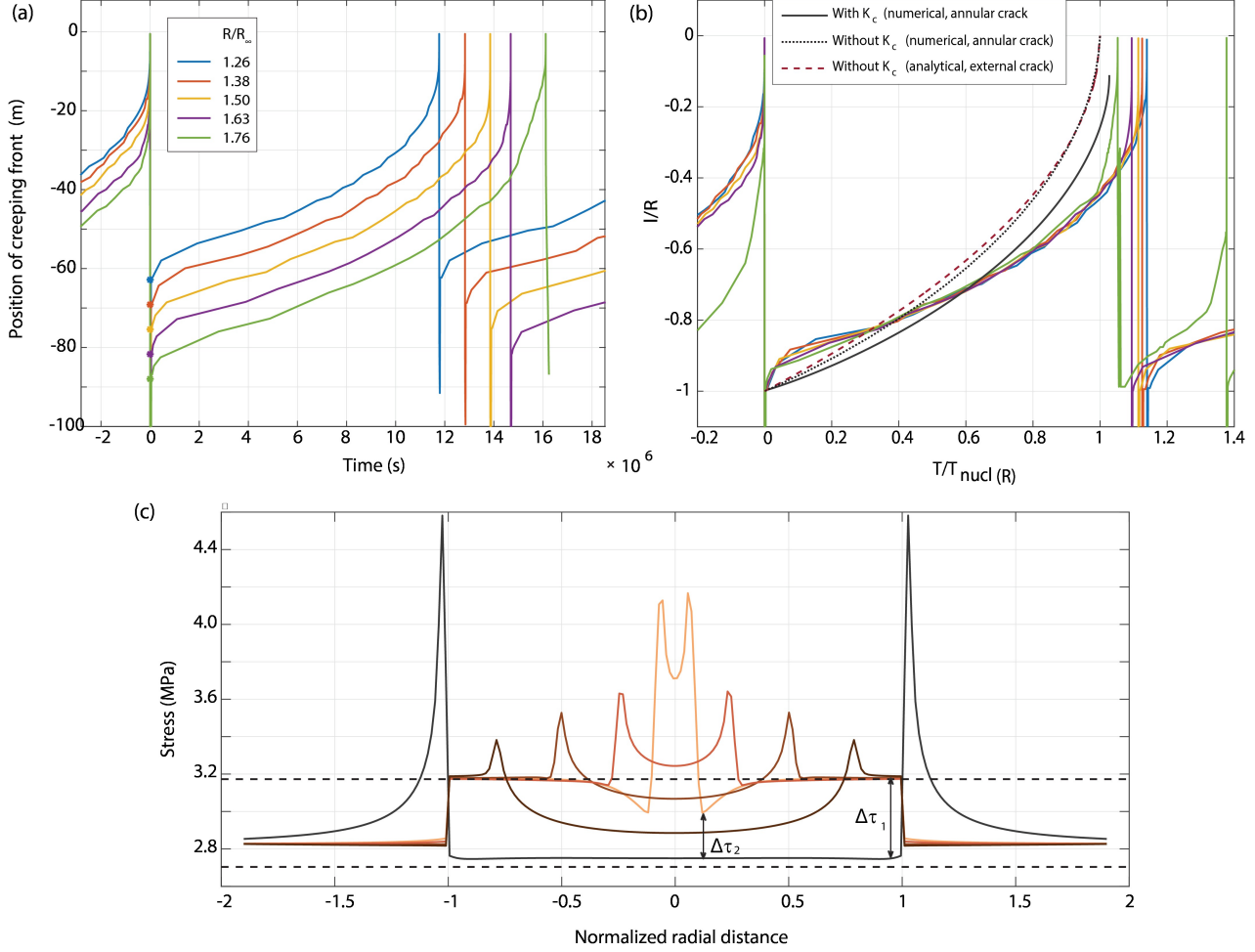


6

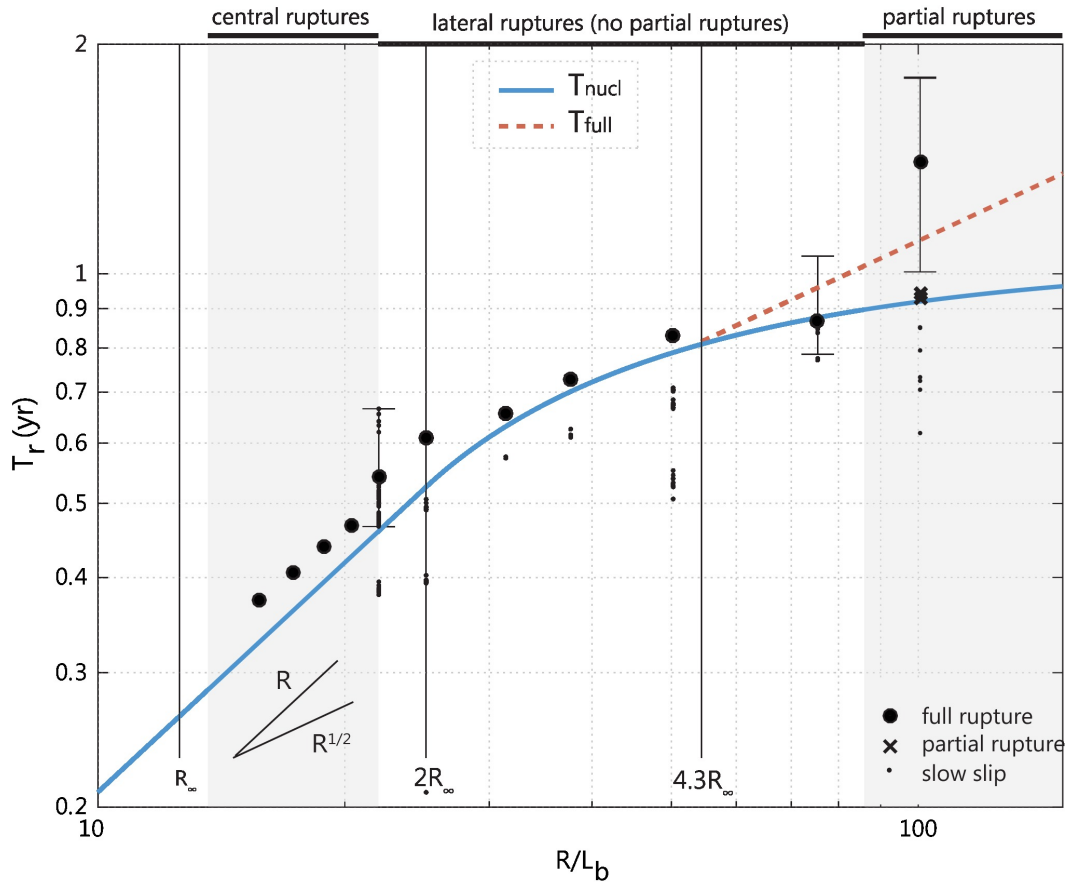
580 **Figure 3.** Scaling of T_r with seismic moment from numerical simulations. The y-axis is the time since the
 581 last rupture; we define T_r as the time between consecutive full ruptures. Error bars indicate range of observed
 582 T_r ; the large variation for the fifth data point is due to alternation of central and lateral ruptures.



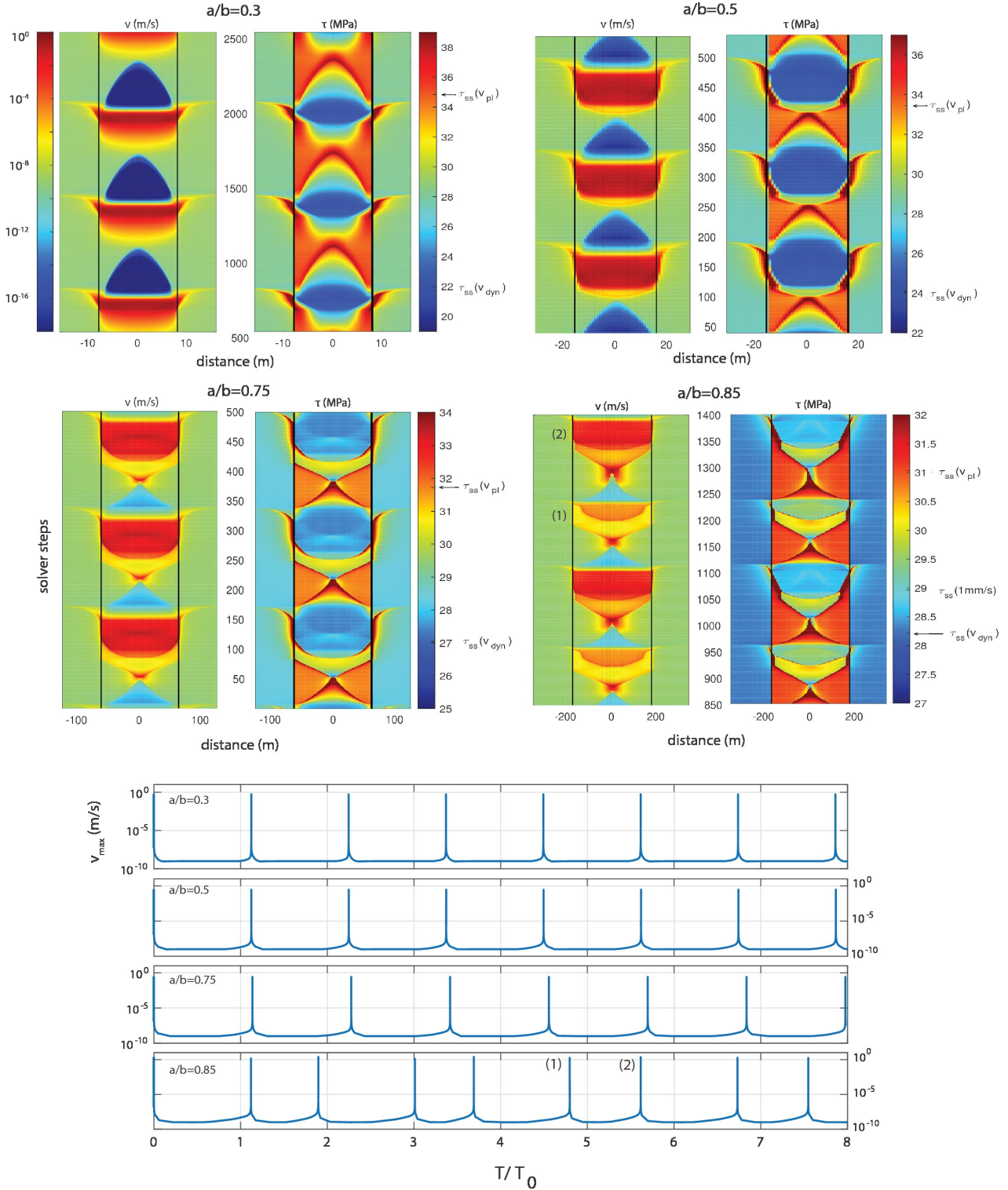
583 **Figure 4.** Scaling of T_r with asperity radius. For aseismic events, we define T_r as the time between peaks
 584 in slip velocity. We denote as “slow slip” brief slow slip events such as those in Fig. 2.



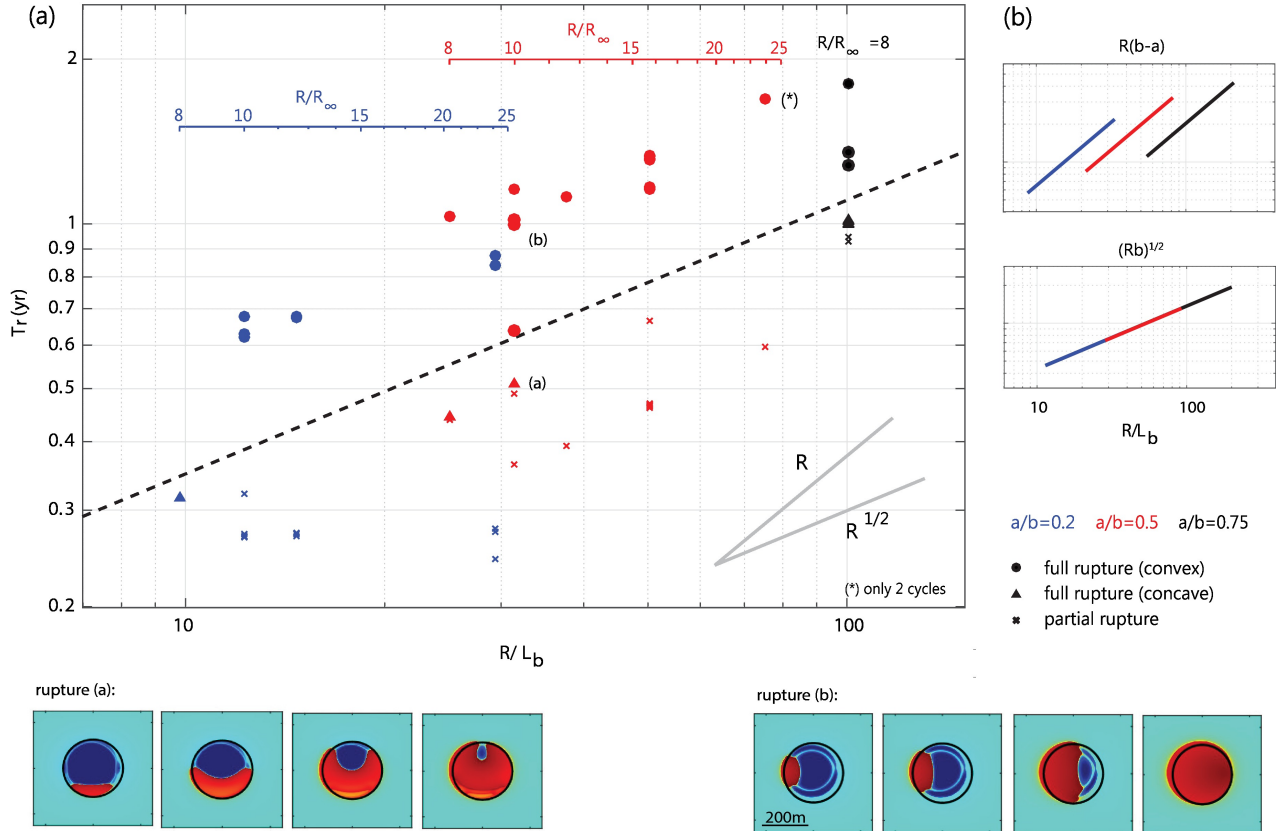
585 **Figure 5.** Top left: Interseismic propagation of creeping front from the edge of the asperity (indicated
 586 by the circle) to the center, estimated from peak stresses. The vertical lines are seismic ruptures. Top right:
 587 Same plot, with the y-axis normalized by asperity radius and the x-axis normalized Eq. 9. The black lines
 588 are the expected propagation of the front (see text), the red dashed line is the approximate solution derived
 589 in Appendix A. Bottom: stress profiles as the creep front propagates inwards. $\Delta\tau_1$ is the difference between
 590 residual stress after an earthquake ($\tau_{ss}(v_{co})$ and ($\tau_{ss}(v_{pl})$), shown by the horizontal dashed lines. As the
 591 creep front approaches $r = 0$, the slip velocity exceeds v_{pl} and the stress difference decreases ($\Delta\tau_2$).



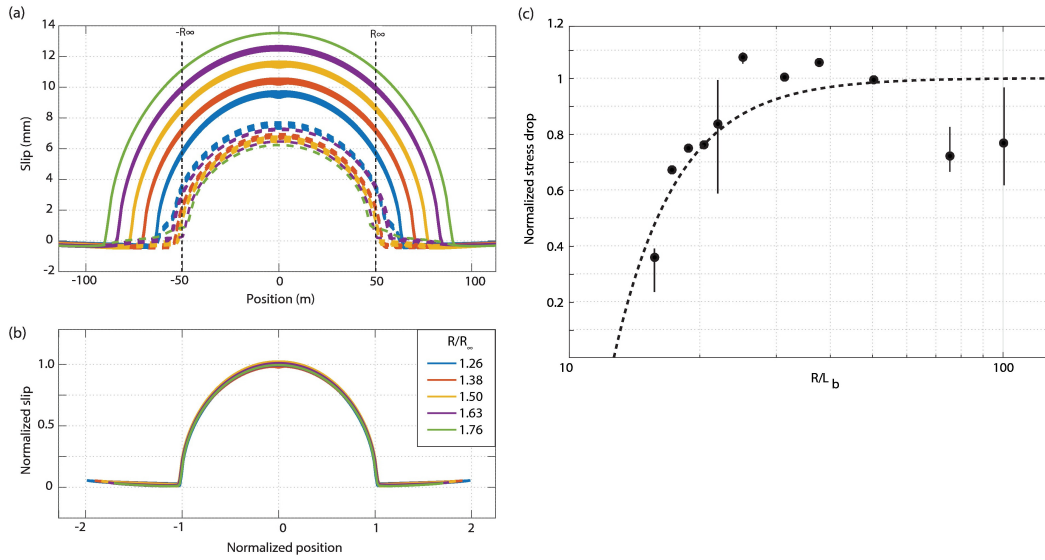
592 **Figure 6.** Scaling of T_r with R from the simulation (dots) and crack models (lines). Vertical lines mark the
 593 expected transition between regimes: aseismic to seismic (R_∞); central rupture to lateral ruptures ($2R_\infty$);
 594 onset of partial ruptures ($4.33R_\infty$), while the transitions observed in the simulations are marked at the top.
 595 T_{nucl} and T_{full} are calculated from eq. 13 and 16.



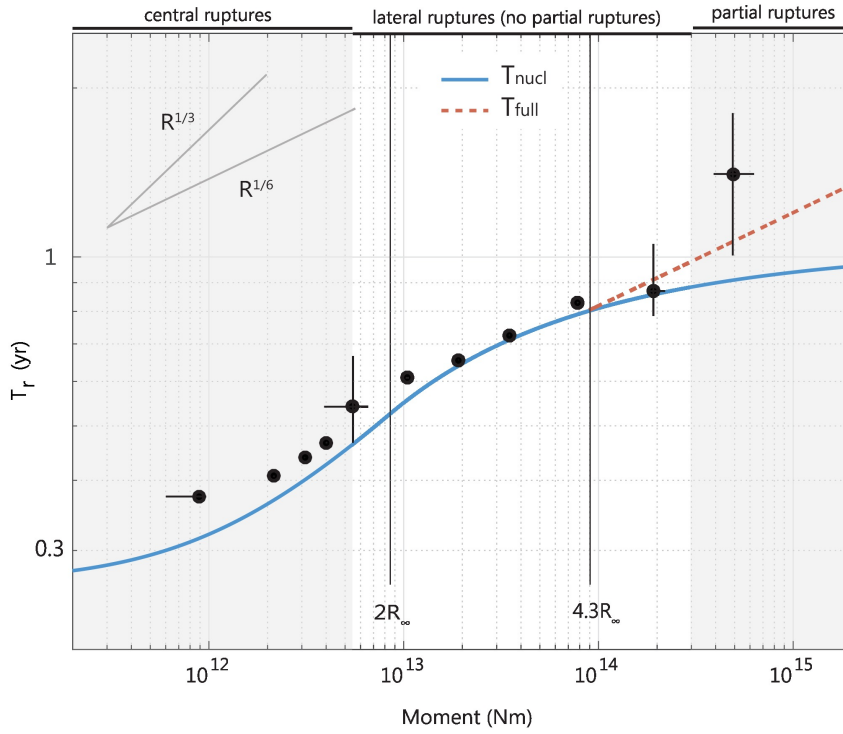
596 **Figure 7.** Top: Cycles for asperities with $R/R_\infty = 1.26$ and variable R and a/b , showing slip velocity
 597 and shear stress. For $a/b = 0.75$ and 0.85 the main quake (reaching the edge of the asperity) is preceded
 598 by brief fast slip. For $a/b = 0.85$, the velocity reached by the subsequent event (and determining the stress
 599 at the beginning of the following cycle) alternates between $\sim 10^{-4} - 10^{-3}$ m/s (event marked as 1) and
 600 ~ 0.1 m/s (event marked as 2). Fast events have a higher stress drop. Bottom: maximum slip velocity vs. time
 601 normalized by T_0 (from eq. 13). Note the period-2 cycle for $a/b = 0.85$, due to the alternation of seismic and
 602 slow events: fast events, with a higher stress drop, are followed by longer cycles.



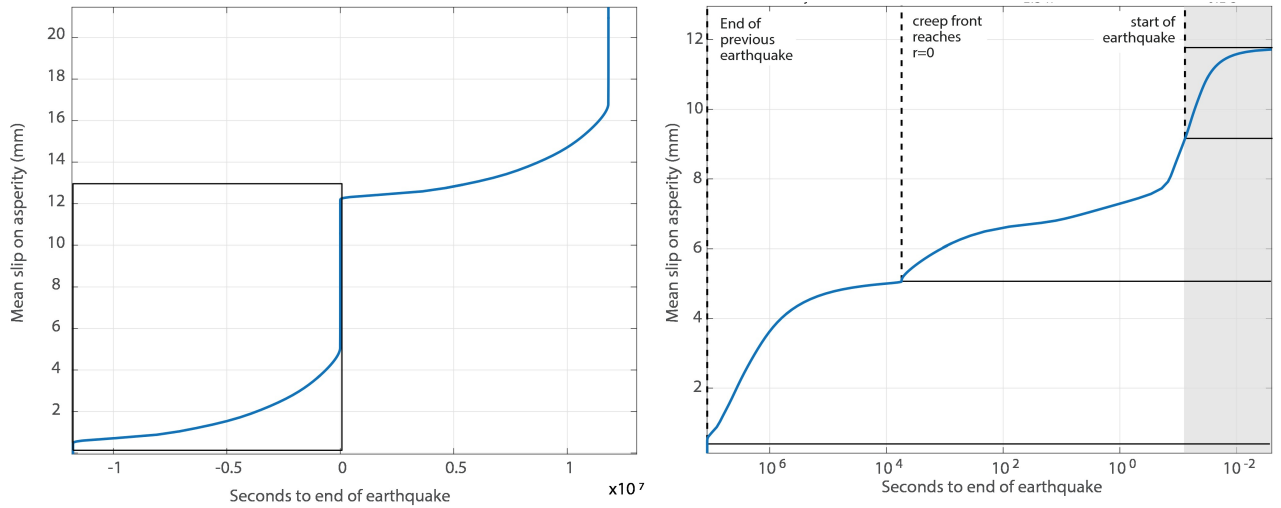
603 **Figure 8.** Scaling for asperities in the partial ruptures regime ($R/R_\infty \geq 8$), with fixed b and variable $b - a$.
 604 (a) Simulated cycles, with different rupture styles: partial ruptures (crosses), full ruptures that start with con-
 605 cave “horseshoe” shape (triangles), and convex full ruptures (circles). (b) Scaling expected from the classic
 606 argument: $T_r \sim R\Delta\tau \sim R(b - a)$ (top), and from the $K_I \geq K_c$ argument ($T_r \sim \sqrt{Rb}$). The simulated
 607 events have different stress drops but the same fracture energy (from eq. A.14), so the $K_I \geq K_c$ argument
 608 predicts that they should fall on the same line.



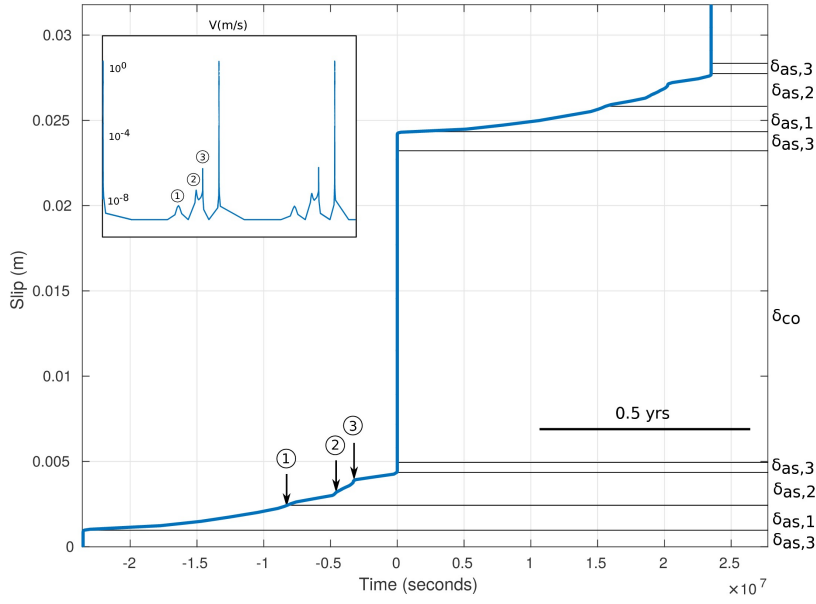
609 **Figure 9.** (a) Slip profiles for central ruptures with respect to the slip at the boundary at the onset of a rup-
 610 ture. Thick lines are the final slip distribution, dotted lines are the slip when the slip speed reaches v_{dyn} (i.e.
 611 at the start of an earthquake). (b) Slip profiles at the end of a seismic event, with lengths normalized by R_{∞} .
 612 (c) Stress drops in the simulations (dots) and expected from eq. 19, which takes into account the aseismic nu-
 613 cleation phase (dotted line). Stress drops are normalized by $\Delta\tau = 4.2$ MPa, which is the stress drop derived
 614 from the slip profile in the simulations and the expected limiting value as $R \gg R_{\infty}$.



615 **Figure 10.** Scaling of T_r vs. M_0 . T_{nucl} and T_{full} from eq. 13, 16 and the seismic moment from eq. 19.
 616 Transitions between rupture styles are determined by R/R_∞ , not moment: depending on physical properties
 617 (a, b and σ) they would occur at different magnitude thresholds.

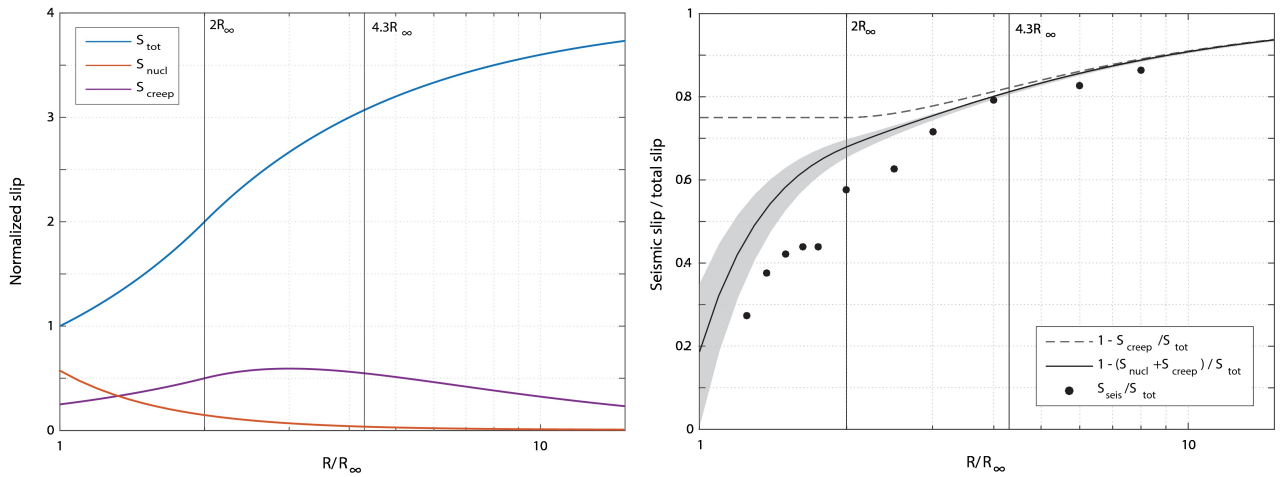


618 **Figure 11.** Average slip on the asperity during the cycle for the fault with $R = 16L_b$. δ_x are labeled as in
 619 Eq. 20.



620

Figure 12. Average slip on the asperity during the cycle for the fault with $R = 50L_b$.



621

Figure 13. Left: slip budget estimated from eq. C.1, C.3 and C.4, normalized by the slip deficit on an

622

asperity with $R = R_\infty$. Right: Fraction of seismic to total slip. Circles indicate the ratios observed in simula-

623

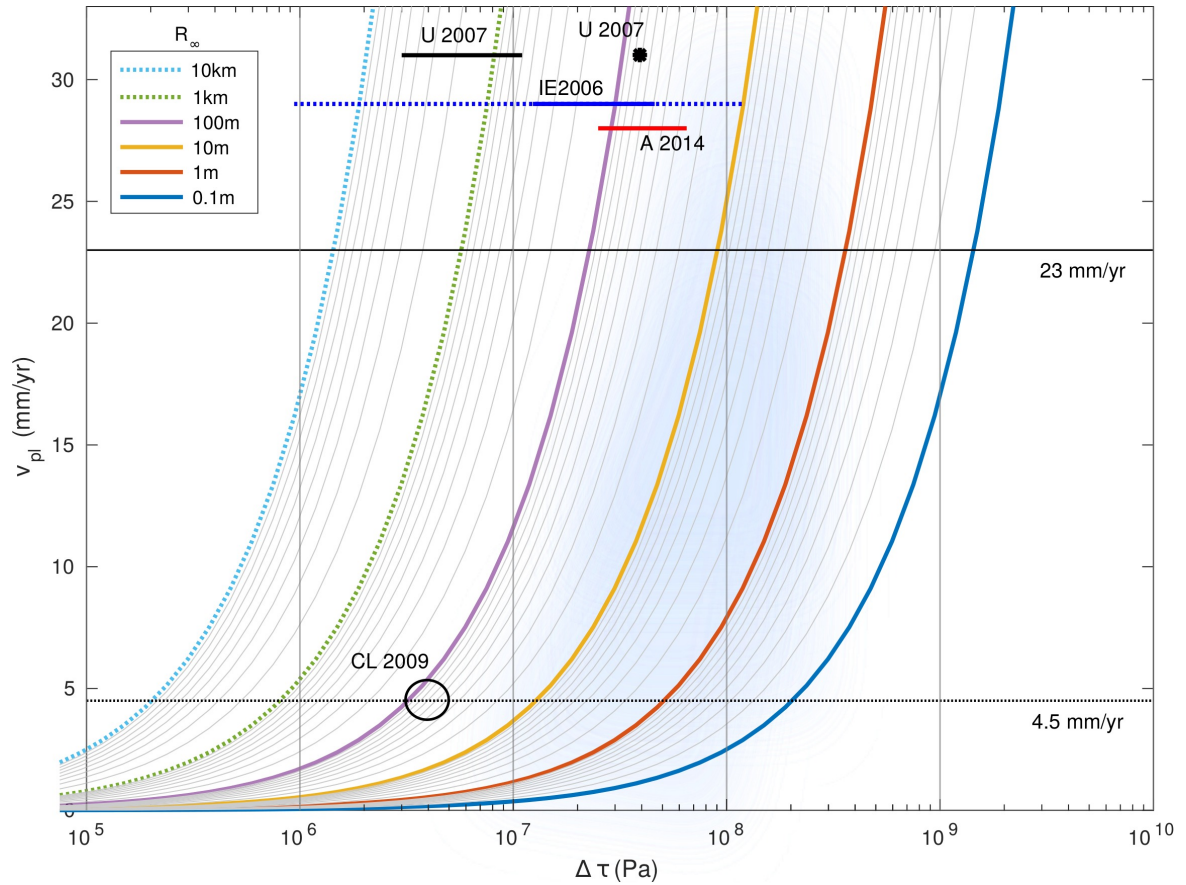
tions; the black line is eq. 21, assuming that $\Delta\tau$ in eq. C.4 is the same as in eq. C.1, C.3. The grey area shows

624

the range obtained allowing the stress drop during nucleation to differ from the stress increase during creep

625

propagation ($\Delta\tau_{nucl} = [0.7 - 1.3]\Delta\tau_{creep}$).



626 **Figure 14.** Combination of creep rate, stress drops and nucleation lengths required to satisfy the scaling
 627 observed at Parkfield according to eq. 28. Each line shows creep rate v_{pl} as a function of stress drop $\Delta\tau$ for
 628 a particular value of R_∞ . The parameters chosen by *Chen and Lapusta* [2009] resulted in $R_\infty \sim 83$ m and
 629 $\Delta\tau \sim 4$ MPa, and the authors inferred a creep rate of 4.5 mm/yr (smaller than the value of 23 mm/yr used
 630 by *Nadeau and Johnson* [1998]). This interpretation is shown by the ellipse marked “CL2009”. Bars at the
 631 top indicate seismological estimates of stress drops: *Abercrombie* [2014] (A2014, Parkfield, showing only
 632 well constrained values); *Imanishi and Ellsworth* [2006] (IE2006, Parkfield, with the entire range shown
 633 by the dotted line and one standard deviation by the thick line). *Uchida et al.* [2007] (U2007, offshore Ka-
 634 maishi, Japan, with the dot marking the value for the $M_w 4.9$ repeater and the bar marking values estimated
 635 for smaller events). The shaded area indicates plausible values of parameter combinations, based on observed
 636 stress drops and nucleation lengths inferred from the small observed magnitudes (see text).

637

A: Creep front propagation

In order to slip at the loading velocity, the stress behind the crack tip must increase from the residual stress after an earthquake $\tau_{ss}(v_{co})$ to the steady-state value at the creep rate $\tau_{ss}(v_{cr})$. In the simulations, we note that this is close to the loading rate v_{pl} , and for simplicity here we assume $v_{cr} = v_{pl}$. The crack can therefore be approximated by superimposing a stress-free end-driven crack and a crack with a spatially uniform negative stress drop $\Delta\tau = \tau_{ss}(v_{pl}) - \tau_{ss}(v_{co})$. Neglecting the contribution from fracture energy, the length of the crack $a(t)$ is determined by the condition that the total stress intensity factor vanishes, or

$$K_I(t, a) = K_{\Delta\tau}(a) \quad (\text{A.1})$$

638

where K_I is the SIF due to displacement at $a \geq R$, which we assume to grow linearly in time ($S = v_{pl}t$). The propagating creep front can be treated as an annular crack driven by edge displacement, which grows in response to a increase in the displacement boundary condition (analogous to the 2-D case analyzed by *Mavrommatis et al.* [2017]). We consider an annular crack with outer radius R and inner radius $a(t)$.

639

640

641

642

643

A.1 Annular Crack

For simplicity, throughout this work we employ results for stress intensity factors for Mode-I cracks; for Mode-II or Mode-III cracks, the stress intensity factors vary by a factor of order 1. Closed form solutions for the stress intensity factors for an annular crack with fixed slip at $r = R$ are, to our knowledge, not available. Therefore we estimate them numerically, and validate these solutions by comparing them to analytical results in the limits: $a \ll R$ and $a \rightarrow R$. Consider an annular crack with inner and outer radii a and R , subject to an axisymmetric stress $\tau(r)$. The SIF can be expressed as

$$K(t, a) = \int_a^R \tau(t, r) k(r) dr \quad (\text{A.2})$$

where $k(r)$ is the SIF for a unit ring force at radius r . We evaluate $k(r)$ numerically, using the method introduced by *Clements and Ang* [1988]. The stress distribution relevant for edge loading K_I is

$$\tau_l(r, t) = \tau_{rd}(r) v_{pl}t \quad (\text{A.3})$$

644

where τ_{rd} is the stress due to a unit ring dislocation at $r = R$ (Fig. B.2), with slip $\delta(r, t)$:

$$\delta(r, t) = \begin{cases} v_{pl}t & r \geq R \\ 0 & r < R \end{cases} \quad (\text{A.4})$$

where t is the time since the last event and v_{pl} the plate velocity. The stress field inside a dislocation ring is given by [Kroupa, 1960]:

$$\tau_{rd}(r) = \frac{\mu' v_{pl} t}{\pi R} \frac{E(\rho)}{1 - \rho^2} \quad (\text{A.5})$$

645 where $\rho = r/R$, and $E(k)$ is the complete elliptic integral of the second kind, which varies
 646 from 1 to $\pi/2$. It can be verified that this form gives the $1/x$ singularity in stress as $r \rightarrow R$
 647 and reduces to $\tau_{rd} = \mu v_{pl} t / 2R$ at $r = 0$. We checked that the numerical solution of $K_l(a)$,
 648 approaches known solutions for the two limiting cases: the result from *Selvadurai and Singh*
 649 [1986] for $a \ll R$, and the 2-D solution for $a \rightarrow R$.

For $K_{\Delta\tau}$, we assume a uniform (and negative) stress drop (Fig. 5), associated with increase in stress from that after dynamic rupture to steady state friction for creep at $v = v_{pl}$, i.e. $\Delta\tau = \tau_{ss}(v_{pl}) - \tau_{ss}(v_{co})$. We neglect the acceleration in slip speed (and hence decrease in $K_{\Delta\tau}$) as the slip front approaches the center (seen in the last snapshot in Fig. 5). We use the approximate solution from *Tada et al.* [2000]:

$$K_{\Delta\tau}(l) = \Delta\tau \sqrt{\frac{\pi l}{2}} \cdot F\left(\frac{l}{R}\right), \quad (\text{A.6})$$

with

$$F\left(\frac{l}{R}\right) = \frac{1 - 0.36 l/R - 0.067(l/R)^2}{\sqrt{1 - l/R}} \quad (\text{A.7})$$

650 and $l = R - a$. Using our numerical solution for $K_l(t, a)$ (obtained through Eq. A.2 and
 651 A.5) and eq. A.6 into eq. A.1, we obtain the equation of motion for the creep front $a(t)$ shown
 652 in Fig. 5.

653 **A.1.1 Calculating T_{nucl}**

To get an analytical approximation for the time required for the creep front to reach the center of the asperity, we consider the limit $a/R \ll 1$. This is an estimate for the nucleation time on asperities with central ruptures. For K_l , we note that the stress intensity factor due to a displacement $\delta = S$ for $r \geq R$ and $\delta = 0$ for $r \leq a$ and zero stress in between is equivalent to that imposed by the boundary conditions $\delta = 0$ for $r \geq R$ and $\delta = -S$ for $r \leq a$, since the second state can be obtained from the first by subtracting a rigid body displacement, which generates no stresses. The stress field outside a dislocation ring of radius a and strength $-S = -v_{pl} T_{nucl}$ is [Kroupa, 1960]

$$\tau_{rd}(r) = \frac{\mu' S}{\pi a} \left[\frac{K(1/\rho)}{\rho} - \frac{\rho E(1/\rho)}{\rho^2 - 1} \right] \quad (\text{A.8})$$

where $\rho = r/a$ and $K(k)$ is the complete elliptic integral of the first kind. As $1/\rho \rightarrow 0$, this becomes:

$$\tau_{rd} = -\frac{v_{pl}\mu'}{2a} \left(\frac{a}{r}\right)^3 T_{nucl} \quad (\text{A.9})$$

for $r > a$. Since we are estimating the time for the creep front to reach the center of the asperity, $a(T_{nucl}) = 0$, we have $a/R \ll 1$ and can approximate the problem as an external crack of radius a . Since the displacements at $r \rightarrow \infty$ for an external crack subject to a field decaying sufficiently rapidly is null, the boundary condition $\delta(R) = 0$ is automatically satisfied in this limit. The SIF for an external crack subject to a stress field of the form $\tau(r) = \tau_0(r/a)^{-n}$ (as in eq. A.9) is given by [Sih, 1973], and for $n = 3$ reduces to

$$K_l = -\frac{2}{\sqrt{\pi}} \tau_0 \sqrt{a} = -\frac{v_{pl}\mu'}{\sqrt{\pi a}} T_{nucl} \quad (\text{A.10})$$

The stress intensity factor for a constant stress drop (eq. A.6) in the limit $a/R \rightarrow 0$ is given by [Tada et al., 2000]

$$K_{\Delta\tau} = \frac{4\Delta\tau R}{\pi^{3/2}} \sqrt{\frac{1-a/R}{a}} \sim \frac{4\Delta\tau R}{\pi^{3/2}\sqrt{a}} \quad (\text{A.11})$$

Neglecting fracture energy, we set $K_l = K_{\Delta\tau}$ and obtain

$$t_0(R) = \frac{4R\Delta\tau}{\pi v_{pl}\mu'} \quad (\text{A.12})$$

654 In the simulations, there is a delay between the arrival of the creep front and the onset
 655 of an earthquake; depending on R , this is of the order of seconds-hours (Fig. 1), and thus neg-
 656 ligible compared to the cycle duration. Therefore we take the nucleation time T_{nucl} equal to
 657 t_0 . We can gain some insight into how the asperity dimension affects creep front propagation
 658 by considering the scaling of K_l and $K_{\Delta\tau}$. Rewriting eq. A.10 in terms of the non-dimensional
 659 length $\tilde{a} = a/R$, we see that $K_l \sim t/\sqrt{R}$, a result which, as we demonstrate in Appendix
 660 B is valid for a crack of any shape within the asperity. Similarly, eq. A.6 shows that $K_{\Delta\tau} \sim$
 661 \sqrt{R} . Therefore, neglecting fracture energy and solving $K_l = K_{\Delta\tau}$ for a given value of \tilde{a} re-
 662 sults in $t \sim R$, so that when both distance and time are normalized by a factor proportional
 663 to R , the creep evolution curves collapse as in fig. 5. Fig. 5 also shows that the normalized
 664 equation of motion is in agreement with the equation of motion calculated numerically.

665 **A.1.2 Effect of fracture energy**

We include the effect of fracture energy by finding numerical solutions of

$$K_l + K_{\Delta\tau} = K_c \quad (\text{A.13})$$

where K_c is the fracture toughness, which is related to the fracture energy by eq. 8. We employ the fracture energy for the aging law, in the no-healing approximation and constant slip velocity v_{in} , as given by [Rubin and Ampuero, 2005]:

$$G_c = \frac{d_c b \sigma}{2} \left[\log \left(\frac{v_{in} \theta_i}{d_c} \right) \right]^2 \quad (\text{A.14})$$

666 Since the crack is propagating into the locked region, we take $\theta_i = t + d_c/v_{co}$ (from eq. 3,
667 with $\dot{\theta} \sim 1$ and $\theta(t=0) = d_c/v_{co}$).

668 **A.2 An approximate solution**

Here we derive an analytical form for the equation of motion of the creep front by treating the annular crack as an external circular crack and approximating the stress field imposed by the ring dislocation at $r = R$. The SIF for an external crack of radius a subject to uniform stress between $r = a$ and $r = R$ is [Sih, 1973]:

$$K_{\Delta\tau} = \frac{2\sqrt{R}}{\sqrt{\pi}} \sqrt{\frac{1-\tilde{a}^2}{\tilde{a}}} \Delta\tau \quad (\text{A.15})$$

with $\tilde{a} = a/R$. Note that this differs from Eq. A.11 due to the use of an external crack, as opposed to an annular crack. Next we approximate K_l as due to a concentrated ring force at $r = R$, i.e. $\tau(r) = P\delta(R)$, where P is a constant; $\delta(x)$ is the Dirac delta function, so that the ring force has the same form as the gradient of the imposed displacement (Eq. A.4). This approximation assumes that the SIF is dominated by the singularity in the stress field; we note that for 2 dimensional cracks, these two loading configurations produce exactly the same SIF ($K_l \sim \sqrt{l}$, where l is the distance between the loading point and the crack tip). The SIF in this case is Sih [1973]

$$K_l = \frac{2P}{\sqrt{\pi R}} \frac{1}{\sqrt{\tilde{a}(1-\tilde{a}^2)}} \quad (\text{A.16})$$

Setting $P = \alpha v_{pl} t$ (so that K_l is proportional to load point displacement), $K_{\Delta\tau} = K_l$ gives

$$a(t) = R \sqrt{1 - \frac{\alpha v_{pl} t}{R}} \quad (\text{A.17})$$

669 Further choosing $\alpha = \dot{r}_c/v_{pl}$ with $\dot{r}_c = \pi\mu'v_{pl}/4\Delta\tau$ matches the condition given by eq. A.12.
670 This solution, although not rigorous, is close to the numerical result (Fig. 5).

671 **B: Estimating $T_{full}(R)$**

672 Eq. 7 considers the contribution of energy from elastic loading (K_l) as well as stress vari-
673 ations within the crack ($K_{\Delta\tau}$). In appendix A, we saw that the propagation of the creep front

674 is controlled by both terms. For a seismic rupture, the problem can be simplified by noting
 675 that we are considering a full seismic cycle, so that the net stress change is null. At $t = 0$
 676 (just after a full rupture) the stress in the asperity is low: $\tau = \tau_{ss}(v_{co})$. Interseismically, creep
 677 outside the asperity raises the applied stress, while frictional strength changes as a result of
 678 healing as well as creeping on part of the asperity. These interseismic stress changes are re-
 679 versed during seismic rupture, since the stress behind the seismic crack tip is $\tau = \tau_{ss}(v_{co})$.
 680 Therefore we can set $K_{\Delta\tau} = 0$. For this argument to be strictly valid, we should account
 681 for stress changes on the asperity due to interseismic slip outside the hypothetical growing rup-
 682 ture. However, for simplicity, here we neglect the contribution from interseismic slip and as-
 683 sume that the asperity is entirely locked (a good approximation for $R \gg R_\infty$).

684 We estimate the stress intensity factor for a rupture nucleating at the edge of an asperity
 685 and propagating into the locked region. For a rupture in 2 dimensions, the stress intensity
 686 factor is a function of position along the front and it changes as the rupture grows. We con-
 687 sider the problem of a crack of an arbitrary shape growing within an asperity.

Rice [1989] developed a theory for calculating stress intensity factors for 2-dimensional cracks in a 3-D medium. For a crack subject to a stress field $\sigma(\mathbf{x})$, the stress intensity factor at position s along the rupture front is given by

$$K_I(s) = \int_{crack} k(\mathbf{x}; s) \sigma(\mathbf{x}) dA \quad (\text{B.1})$$

with

$$k(\mathbf{x}; s) = \frac{\sqrt{2\rho(\mathbf{x})} W(\mathbf{x}; s)}{\sqrt{\pi^3} D^2(\mathbf{x}; s)} \quad (\text{B.2})$$

where ρ is the minimum distance between \mathbf{x} and the edge of the crack, D the distance between \mathbf{x} and point s along the crack, and $W(\rho, D)$ a non-dimensional factor which takes into account the crack shape (see Fig. B.1). The terms $k(\mathbf{x}; s)$ are weight functions: they depend on the crack geometry and not on the applied stress. Note that they are a function of position along the front, and they vary as the rupture grows and potentially changes shape. The applied stress field $\sigma(\mathbf{x})$ is determined by the loading conditions on the asperity (i.e. interseismic loading), and is given by eq. A.5. We can now write the stress intensity factor in terms of non-dimensional variables $\xi = r/R$, $\tilde{\rho} \equiv \rho/R$ and $\tilde{D} \equiv D/R$:

$$K_I(s) = \frac{\mu' v_{pl} t}{\sqrt{R}} \phi(s) \quad (\text{B.3})$$

with

$$\phi(s) = \int \frac{\sqrt{2\tilde{\rho}(\mathbf{x})} W(\mathbf{x}; s)}{\sqrt{\pi^3} \tilde{D}(\mathbf{x}; s)^2} \frac{E(\xi)}{1 - \xi^2} d\tilde{A} \quad (\text{B.4})$$

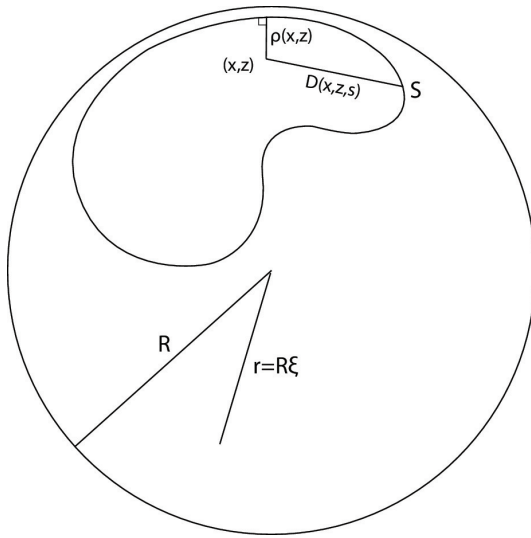
where the integration is over the rescaled crack. Note that this term only depends on normalized lengths. As the crack grows and changes shape, the quantities and $\tilde{\rho}$, \tilde{D} and W vary. A rupture stops when $K_l(s) < K_c$ for all points s which are still within the velocity weakening region (or after penetrating a short distance into the VS region). For easier notation, we drop the dependence on s and we simply write $K_l < K_c$ when referring to this condition. A first order scaling between the stress intensity factor and the asperity size can be derived by assuming that ϕ does not depend on R . This implies that rupture evolution is independent of asperity dimension, i.e. the rupture history on an asperity is simply a rescaled version of the rupture history on an asperity of a different size. This can be considered an acceptable first-order approximation given that $\tilde{\rho}$, \tilde{D} must always be in the range $[0, 2]$. By setting Eq. B.3 equal to K_c we obtain an estimate of the minimum recurrence interval:

$$T_{full} = \frac{K_c \sqrt{R}}{\phi \mu' v_{pl}} \quad (\text{B.5})$$

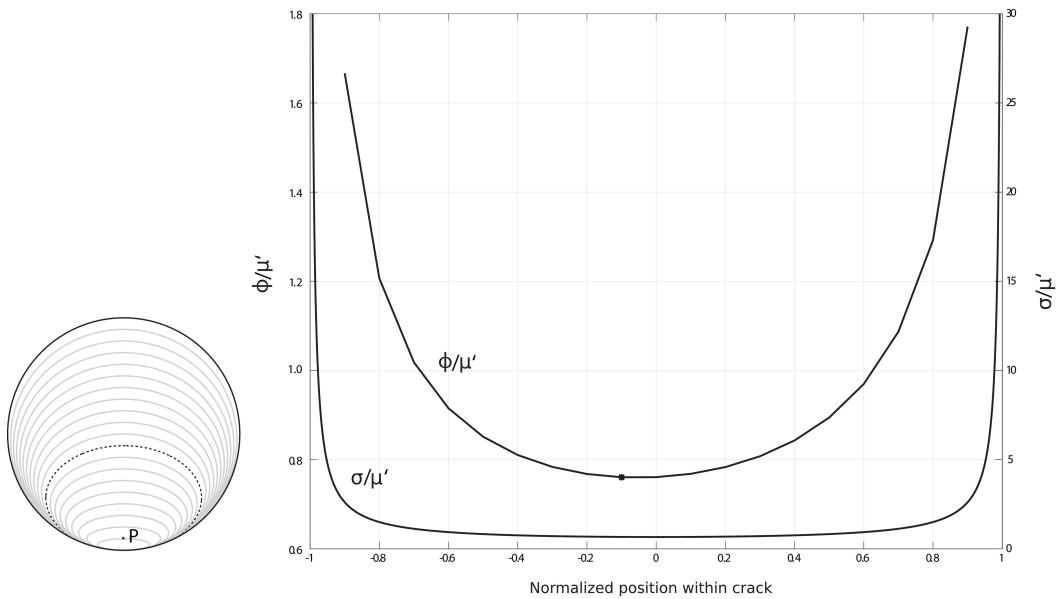
688 and with constant ϕ we find a square-root scaling between recurrence interval and source di-
689 mension.

690 To estimate realistic values of $T_{full}(R)$, we compute ϕ numerically for the rupture his-
691 tory shown in Fig. B.2, using the values of $W(\mathbf{x}; s)$ for an elliptical crack [Wang *et al.*, 1998].
692 In this case K varies along the rupture front. For the innermost point along the rupture front
693 (P), we note that the ϕ has a non-monotonic behavior as the rupture dimension grows: as P
694 moves towards the center of the asperity, the stress field near P decreases and so does $\phi(P)$.
695 Note that the minimum of K occurs before P reaches the center of the asperity, since $\phi(P)$
696 does not depend only on the stress at P but also on the crack size (it increases with crack di-
697 mension). The minimum value of ϕ is 0.76.

698 The behavior of stress intensity factor at one point is not enough to determine whether
699 the rupture stops. However, this simple model shows that ruptures starting at the edge of an
700 asperity and propagating down a stress gradient may encounter a minimum SIF as they grow.
701 This may lead to either partial seismic ruptures, or slow slip episodes, depending on whether
702 the minimum is encountered before or after reaching the critical nucleation dimension.



703 **Figure B.1.** Example of a rupture propagating within the asperity, as presented in *Rice* [1989]. The dimen-
 704 sions relevant to the calculation of stress intensity factors (Eq. B.2) are marked.



705 **Figure B.2.** Stress intensity factor for a rupture nucleating on the side. Left: sequence of elliptical cracks
 706 representing an idealized rupture history. Each ellipse is obtained by shifting the center along the vertical and
 707 matching the asperity curvature at the point of contact. Right: Stress intensity factor and stress field within the
 708 asperity. The stress intensity factor is calculated at point P (left panel). The minimum in ϕ (0.76) is marked
 709 with a circle, and it corresponds to the dotted ellipse in the left panel.

710 **C: Slip budget**

711 The slip deficit at the time of the first nucleation is given by $v_{pl}T_{nucl}$, and from eq. 13
712 we have

$$S_{tot} = \begin{cases} \frac{4\Delta\tau}{\pi\mu'} R & R < 2R_\infty \\ \frac{16\Delta\tau}{\pi\mu'} R_\infty \left(1 - \frac{R_\infty}{R}\right) & R \geq 2R_\infty. \end{cases} \quad (C.1)$$

713 In order to calculate the average slip from the propagation of the creep front, we need
714 to know the slip profile for an annular crack analyzed in section A. While there are simple ex-
715 pressions for this problem for 1D cracks, there are no closed form solutions for the annular
716 crack. Therefore we use the following approximation: points ahead of the creep front don't
717 slip, and points behind it accumulate slip at a constant rate v_{cr} (which, as discussed earlier,
718 is of the order of v_{pl}). At the time of nucleation, the total slip at a point of radius r is $v_{cr}(T_{nucl} - t(r))$,
719 where $t(r)$ is the time when the front reached r . Approximating this time by the inverse of
720 eq. A.17, we obtain

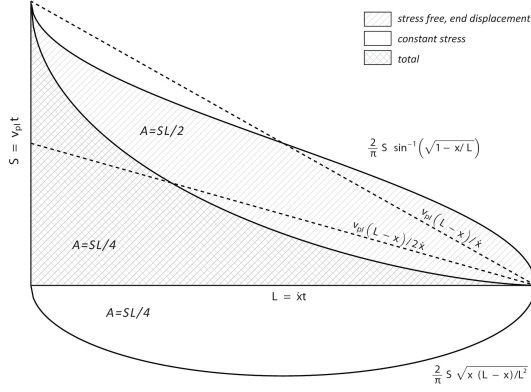
$$s_{creep}(r) = \begin{cases} \frac{4\Delta\tau}{\pi\mu'} \frac{v_{cr}}{v_{pl}} \frac{r^2}{R} & R < 2R_\infty \\ \frac{4\Delta\tau}{\pi\mu'} \frac{v_{cr}}{v_{pl}} \frac{r^2 - (R - 2R_\infty)^2}{R} & R \geq 2R_\infty, \end{cases} \quad (C.2)$$

721 We integrate this expression to obtain the average slip on the asperity at the time of nucleation:

$$S_{creep} = \begin{cases} \frac{2\Delta\tau}{\pi\mu'} \frac{v_{cr}}{v_{pl}} R & R < 2R_\infty \\ \frac{32\Delta\tau}{\pi\mu'} \frac{v_{cr}}{v_{pl}} \frac{R_\infty^2}{R} \left(1 - \frac{R_\infty}{R}\right)^2 & R \geq 2R_\infty. \end{cases} \quad (C.3)$$

722 To constrain v_{cr}/v_{pl} , we consider the initial phase of the creep front propagation, when the
723 annulus can be treated as a 1D crack. As shown in Fig. C.1, the average slip within a stress
724 free crack driven by a slip boundary condition is the same as that of a linear slip profile given
725 by constant slip rate $v_{cr} = v_{pl}$. However, the (negative) stress drop crack that cancels the
726 stress intensity factor contributes negative slip, equal to half of the average slip for the stress
727 free crack. Therefore we match the correct average slip in the annulus by setting $v_{cr} = v_{pl}/2$;
728 v_{cr} should be thought of as an average slip velocity.

Finally, we consider the slip accumulated during the nucleation phase by treating the nu-
cleating patch as constant stress drop crack of radius R_∞ (cf. section 6). The average slip due



732 **Figure C.1.** Slip profile for a stress free crack with a displacement boundary condition; the constant stress
 733 drop crack which negates the SIF from the displacement driven crack; and their combination. The dotted
 734 lines are the slip profiles assuming $v = 0$ ahead of the crack tip, and $v = v_{cr}$ behind, with $v_{cr} = v_{pl}$ and
 735 $v_{cr} = v_{pl}/2$.

to this crack embedded within an asperity of radius R is given by

$$S_{nucl} = \frac{16\Delta\tau}{7\pi\mu'} \frac{R_\infty^3}{R^2} \quad (C.4)$$

729 Assuming, as done before, that the stress drops during nucleation and creep propaga-
 730 tion have the same absolute value, $\Delta\tau$ is the same in eq. C.1, C.3, C.4, and these values dif-
 731 fer only by factors containing R and R_∞ .

736 References

- 737 Abercrombie, R. E. (2014), Stress drops of repeating earthquakes on the San An-
 738 dreas Fault at Parkfield, *Geophysical Research Letters*, *41*(24), 8784–8791, doi:
 739 10.1002/2014GL062079.
- 740 Abercrombie, R. E., P. Poli, and S. Bannister (2017), Earthquake directivity, orientation,
 741 and stress drop within the subducting plate at the Hikurangi margin, New Zealand,
 742 *Journal of Geophysical Research*, doi:10.1002/2017JB014935.
- 743 Beeler, N. M., D. L. Lockner, and S. H. Hickman (2001), A simple stick-slip and creep-
 744 slip model for repeating earthquakes and its implication for microearthquakes at Park-
 745 field, *Bulletin of the Seismological Society of America*, *91*(6).
- 746 Blanpied, M. L., C. J. Marone, D. A. Lockner, J. D. Byerlee, and D. P. King (1998),
 747 Quantitative measure of the variation in fault rheology due to fluid-rock interactions,

- 748 *Journal of Geophysical Research*, doi:10.1029/98JB00162.
- 749 Boatwright, J. (2007), The persistence of directivity in small earthquakes, *Bulletin of the*
750 *Seismological Society of America*, 97(6), 1850–1861, doi:10.1785/0120050228.
- 751 Calderoni, G., A. Rovelli, Y. Ben-Zion, and R. Di Giovambattista (2015), Along-strike
752 rupture directivity of earthquakes of the 2009 L'Aquila, central Italy, seismic sequence,
753 *Geophysical Journal International*, 203(1), 399–415, doi:10.1093/gji/ggv275.
- 754 Chen, K. H., R. M. Nadeau, and R. J. Rau (2007), Towards a universal rule on the recur-
755 rence interval scaling of repeating earthquakes?, *Geophysical Research Letters*, 34(16),
756 doi:10.1029/2007GL030554.
- 757 Chen, K. H., R. J. Rau, and J. C. Hu (2009), Variability of repeating earthquake behav-
758 ior along the Longitudinal Valley fault zone of eastern Taiwan, *Journal of Geophysical*
759 *Research*, 114(5), doi:10.1029/2007JB005518.
- 760 Chen, T. (2012), Part I: Structure of central and southern Mexico from velocity and at-
761 tenuation tomography ; Part II: Physics of small repeating earthquakes, Ph.D. thesis,
762 California Institute of Technology.
- 763 Chen, T., and N. Lapusta (2009), Scaling of small repeating earthquakes explained by
764 interaction of seismic and aseismic slip in a rate and state fault model, *Journal of Geo-*
765 *physical Research*, 114, 1–12, doi:10.1029/2008JB005749.
- 766 Clements, D. L., and W. T. Ang (1988), Stress intensity factors for the circular annulus
767 crack, *International Journal of Engineering Science*, 26(4), 325–329, doi:10.1016/0020-
768 7225(88)90112-7.
- 769 Dieterich, J. H. (1978), Time-dependent friction and the mechanics of stick-slip, *Pure and*
770 *Applied Geophysics*, 116(4-5), 790–806, doi:10.1007/BF00876539.
- 771 Dieterich, J. H. (1992), Earthquake nucleation on faults with rate-and state-dependent
772 strength, *Tectonophysics*, 211(1-4), 115–134, doi:10.1016/0040-1951(92)90055-B.
- 773 Eshelby, J. (1957), Determination of the elastic field of an ellipsoidal inclusion, and re-
774 lated problems, *Proceedings of the Royal Society of London*, doi:10.1098/rspa.1957.0133.
- 775 Freund, L. B. (1990), *Dynamic Fracture Mechanics*, Cambridge Monographs on Mechan-
776 ics, doi:DOI: 10.1017/CBO9780511546761.
- 777 Griffith, A. A. (1921), The phenomena of rupture and flow in solids, *Philosophical*
778 *Transactions of the Royal Society A: Mathematical, Physical and Engineering Sciences*,
779 221(582-593), 163–198, doi:10.1098/rsta.1921.0006.

- 780 Harris, R. A., and P. Segall (1987), Detection of a locked zone at depth on the Parkfield,
781 California, segment of the San Andreas fault (USA)., *Journal of Geophysical Research*,
782 92(B8), 7945–7962, doi:10.1029/JB092iB08p07945.
- 783 Hawthorne, J. C., M. Simons, and J. P. Ampuero (2016), Estimates of aseismic slip as-
784 sociated with small earthquakes near San Juan Bautista, CA, *Journal of Geophysical*
785 *Research*, 121(11), 8254–8275, doi:10.1002/2016JB013120.
- 786 Herrendorfer, R., Y. van Dinther, T. Gerya, and L. A. Dalguer (2015), Earthquake supercyc-
787 cle in subduction zones controlled by the width of the seismogenic zone, *Nature Geosci*,
788 8(6), 471–474, doi:10.1038/ngeo2427.
- 789 Imanishi, K., and W. L. Ellsworth (2006), Source scaling relationships of mi-
790 croearthquakes at Parkfield, CA, determined using the SAFOD pilot hole seismic array,
791 in *Geophysical Monograph Series*, vol. 170, pp. 81–90, doi:10.1029/170GM10.
- 792 Irwin, G. (1957), Analysis of Stresses and Strains Near the End of a Crack Traversing a
793 Plate, *Journal of Applied Mechanics*, 24(Sep), 361–364, doi:no DOI.
- 794 Kammer, D. S., M. Radiguet, J. P. Ampuero, and J. F. Molinari (2015), Linear elastic
795 fracture mechanics predicts the propagation distance of frictional slip, *Tribology Letters*,
796 57(3), doi:10.1007/s11249-014-0451-8.
- 797 Kaneko, Y., and P. M. Shearer (2014), Seismic source spectra and estimated stress drop
798 derived from cohesive-zone models of circular subshear rupture, *Geophysical Journal*
799 *International*, 197(2), 1002–1015, doi:10.1093/gji/ggu030.
- 800 Kaneko, Y., and P. M. Shearer (2015), Variability of seismic source spectra, estimated
801 stress drop, and radiated energy, derived from cohesive-zone models of symmetrical and
802 asymmetrical circular and elliptical ruptures, *Journal of Geophysical Research B: Solid*
803 *Earth*, 120(2), 1053–1079, doi:10.1002/2014JB011642.
- 804 Kato, N. (2012a), Fracture energies at the rupture nucleation points of large inter-
805 plate earthquakes, *Earth and Planetary Science Letters*, 353-354, 190–197, doi:
806 10.1016/j.epsl.2012.08.015.
- 807 Kato, N. (2012b), Dependence of earthquake stress drop on critical slip-
808 weakening distance, *Journal of Geophysical Research: Solid Earth*, 117(1), doi:
809 10.1029/2011JB008359.
- 810 Kato, N. (2014), Deterministic chaos in a simulated sequence of slip events on a
811 single isolated asperity, *Geophysical Journal International*, 198(2), 727–736, doi:
812 10.1093/gji/ggu157.

- 813 Kroupa, F. (1960), Circular edge dislocation loop, *Czechoslovak Journal of Physics*, *10*(4),
814 284–293, doi:10.1007/BF02033533.
- 815 Lapusta, N. (2003), Nucleation and early seismic propagation of small and large events
816 in a crustal earthquake model, *Journal of Geophysical Research*, *108*, 1–18, doi:
817 10.1029/2001JB000793.
- 818 Madariaga, R. (1977), High frequency radiation from crack (stress drop) models of earth-
819 quake faulting, *Geophysical Journal of the Royal Astronomical Society*, *51*(3), 625–651,
820 doi:10.1111/j.1365-246X.1977.tb04211.x.
- 821 Materna, K., T. Taira, and R. Bürgmann (2018), Aseismic Transform Fault Slip at the
822 Mendocino Triple Junction From Characteristically Repeating Earthquakes, *Geophysical*
823 *Research Letters*, *45*(2), 699–707, doi:10.1002/2017GL075899.
- 824 Mavrommatis, A. P., P. Segall, and K. M. Johnson (2017), A physical model for interseis-
825 mic erosion of locked fault asperities, *Journal of Geophysical Research: Solid Earth*,
826 *122*(10), 8326–8346, doi:10.1002/2017JB014533.
- 827 Nadeau, R. M., and L. R. Johnson (1998), Seismological studies at Parkfield VI: Mo-
828 ment release rates and estimates of source parameters for small repeating earthquakes,
829 *Bulletin of the Seismological Society of America*, *88*(3).
- 830 Noda, H., and T. Hori (2014), Under what circumstances does a seismogenic patch pro-
831 duce aseismic transients in the later interseismic period?, *Geophysical Research Letters*,
832 doi:10.1002/2014GL061676.
- 833 Rice, J. (1989), Weight function theory for three-dimensional elastic crack analysis, in
834 *Fracture Mechanics: Perspectives and Directions (Twentieth Symposium)*, STP18819S,
835 *ASTM International*, pp. 29–57.
- 836 Rice, J. R. (1993), Spatio-temporal complexity of slip on a fault, *Journal of Geophysical*
837 *Research*, *98*(B6), 9885, doi:10.1029/93JB00191.
- 838 Rubin, A. M., and J. Ampuero (2005), Earthquake nucleation on (aging) rate and state
839 faults, *Journal of Geophysical Research*, *110*(2), 1–24, doi:10.1029/2005JB003686.
- 840 Ruina, A. (1983), Slip instability and state variable friction law, *J. Geophys. Res.*, *88*,
841 10,359–10,370, doi:10.1029/JB088iB12p10359.
- 842 Sammis, C. G., and J. R. Rice (2001), Repeating earthquakes as low-stress-drop events at
843 a border etween locked and creeping fault patches, *Bulletin of the Seismological Society*
844 *of America*, *91*(3), 532–537, doi:10.1785/0120000075.

- 845 Sato, T., and T. Hirasawa (1973), Body wave spectra from propagating shear cracks,
846 *Journal of Physics of the Earth*, 21, 415–431, doi:10.4294/jpe1952.21.415.
- 847 Segall, P. (2010), *Earthquake and Volcano deformation*, 517 pp., doi:
848 10.1002/0471743984.vse7429.
- 849 Segall, P., and A. M. Bradley (2012), Slow-slip evolves into megathrust earthquakes in 2D
850 numerical simulations, *Geophys. Res. Lett.*, 39, 2–6, doi:10.1029/2012GL052811.
- 851 Selvadurai, A. P. S., and B. M. Singh (1986), The axial displacement of a disc inclusion
852 embedded in a penny-shaped crack, *ZAMP Zeitschrift fuer angewandte Mathematik und*
853 *Physik*, 37(1), 64–77, doi:10.1007/BF00955519.
- 854 Sih, G. C. (1973), *Handbook of Stress-intensity Factors*, Bethlehem, Pa., Lehigh Univer-
855 sity.
- 856 Tada, H., P. C. Paris, and G. R. Irwin (2000), *The Stress Analysis of Cracks Handbook*, 58
857 pp., Del Research Corp, Hellertown PA, doi:10.1115/1.801535.
- 858 Turner, R. C., M. Shirzaei, R. M. Nadeau, and R. Bürgmann (2015), Slow and Go: Puls-
859 ing slip rates on the creeping section of the San Andreas Fault, *Journal of Geophysical*
860 *Research: Solid Earth*, 120(8), 5940–5951, doi:10.1002/2015JB011998.
- 861 Uchida, N., T. Matsuzawa, A. Hasegawa, and T. Igarashi (2003), Interplate quasi-static
862 slip off Sanriku, NE Japan, estimated from repeating earthquakes, *Geophysical Research*
863 *Letters*, 30(15), doi:10.1029/2003GL017452.
- 864 Uchida, N., T. Matsuzawa, S. Hirahara, and A. Hasegawa (2006), Small repeating earth-
865 quakes and interplate creep around the 2005 Miyagi-oki earthquake (M=7.2), *Earth,*
866 *Planets and Space*, 58(12), 1577–1580, doi:10.1186/BF03352664.
- 867 Uchida, N., T. Matsuzawa, W. L. Ellsworth, K. Imanishi, T. Okada, and A. Hasegawa
868 (2007), Source parameters of a M4.8 and its accompanying repeating earthquakes off
869 Kamaishi, NE Japan: Implications for the hierarchical structure of asperities and earth-
870 quake cycle, *Geophysical Research Letters*, 34(20), doi:10.1029/2007GL031263.
- 871 Uchida, N., T. Matsuzawa, W. L. Ellsworth, K. Imanishi, K. Shimamura, and
872 A. Hasegawa (2012), Source parameters of microearthquakes on an interplate asperity
873 off Kamaishi, NE Japan over two earthquake cycles, *Geophysical Journal International*,
874 189(2), 999–1014, doi:10.1111/j.1365-246X.2012.05377.x.
- 875 Wang, X., S. B. Lambert, and G. Glinka (1998), Approximate weight functions for
876 embedded elliptical cracks, *Engineering Fracture Mechanics*, 59(3), 381–392, doi:
877 10.1016/S0013-7944(97)00139-2.

- 878 Werner, M., and A. Rubin (2013), Mechanical Erosion of the Seismogenic Zone by Creep
879 from below on Rate-and-State Faults, in *AGU Fall Meeting Abstracts*, San Francisco.
- 880 Wu, Y., and X. Chen (2014), The scale-dependent slip pattern for a uniform fault model
881 obeying the rate- and state-dependent friction law, *Journal of Geophysical Research:*
882 *Solid Earth*, 119(6), 4890–4906, doi:10.1002/2013JB010779.